Han, Y., Mahlstedt, N., Horsfield, B. (2015): The Barnett Shale: Compositional fractionation associated with intraformational petroleum migration, retention and expulsion. - *AAPG Bulletin*, *99*, pp. 2173—2202.

DOI: http://doi.org/10.1306/06231514113

# The Barnett Shale: Compositional fractionation associated with intraformational petroleum migration, retention, and expulsion

**Yuanjia Han, Nicolaj Mahlstedt, and Brian Horsfield**

## ABSTRACT

The Marathon 1 Mesquite well was drilled in Hamilton County, Texas, targeting the Barnett Shale with late oil window maturity. Combining a large suite of petrologic and high-resolution organic geochemical analyses on 120 core samples, we have been able to document qualitatively and quantitatively the effects of petroleum retention and expulsion within and from five intervals within the Barnett Shale. Lithological heterogeneities control the composition and amount of retained fluids; the sorption of oil by solid organic matter is important in all intervals. Applying empirical formulas, we have been able to demonstrate not only that retention is primarily controlled by total organic carbon (TOC), but also that the "live" or "labile" component, rather than "dead" or "inert" carbon, constitutes the most active sorptive sites. Additional retention in the micropores provided by biogenic microcrystalline quartz (sponge spicules) accounts for the sweet spot defined by an "oil crossover" in the 914-m (30-ft) thick second interval. The fluorescing oil occurring in the axial chamber of the sponge spicules and that sorbed on organic particles are together enriched in saturated hydrocarbons, whereas the dispersed oil from the adjacent interval 3 is depleted in this compound class. Mass-balance calculations reveal that short-distance migration of petroleum into this "reservoir" interval (second) fractionates the generated oil into a higher quality oil by preferential retention in the order polar compounds > aromatic hydrocarbons > saturated hydrocarbons within the underlying organic matter and clay-rich third interval



Manuscript received June 22, 2014; provisional acceptance October 23, 2014; revised manuscript received March 11, 2015; final acceptance June 23, 2015.
DOI: 10.1306/06231514113

**AUTHORS**

YUANJIA HAN ~ *Section 4.3 Organic Geochemistry, German Research Centre for Geosciences (GFZ), Telegrafenberg, Potsdam 14473, Germany; yuanjia@gfz-potsdam.de*

Yuanjia Han received his B.S. and M.S. degrees from China University of Geosciences in 2010 and 2012, respectively. He is currently a Ph.D. student at the German Research Centre for geosciences under the auspices of the Technical University of Berlin. His research interests focus on the mechanisms of hydrocarbon retention and migration in unconventional shale reservoirs.

NICOLAJ MAHLSTEDT ~ *Section 4.3 Organic Geochemistry, German Research Centre for Geosciences (GFZ), Telegrafenberg, Potsdam 14473, Germany; nicolaj.mahlstedt@gfz-potsdam.de*

Nicolaj Mahlstedt is a postdoc at the German Research Centre for Geosciences. He studied applied geosciences and holds a diploma and Ph.D. from the Technical University of Berlin. He conducted his Ph.D. within the GFZ-Industry-Partnership-Program investigating "High Temperature Methane" generation. His major scientific interests include petroleum system analysis, oil and gas retention processes, compositional kinetic modeling, and the development of geochemical screening tools.

BRIAN HORSFIELD ~ *Section 4.3 Organic Geochemistry, German Research Centre for Geosciences (GFZ), Telegrafenberg, Potsdam 14473, Germany; horsf@gfz-potsdam.de*

Brian Horsfield is a full professor of organic geochemistry and hydrocarbon systems at the Technical University of Berlin, Germany, as well as leader of organic geochemistry at the German Research Centre for Geosciences. He is a member of the German Academy of Science and Technology. He has more than 30 yr experience working with and for industry in upstream research and development. The evaluation of gas-in-place and producibility in unconventional hydrocarbon systems of the United States,

South Africa, China, Australia, and North Africa are key activities in service and research at the present time.


## ACKNOWLEDGEMENTS

We wish to thank D. M. Jarvie and R. J. Hill for their careful reviews and helpful comments. The editorial comments and suggestions by Terrilyn Olson are also gratefully acknowledged. Parts of this study were carried out during the course of the "GASH–Gas Shales in Europe" initiative. The authors wish to thank the sponsors of this project, especially Marathon Petroleum Corporation, for providing sample material. We are also grateful to Prof. Andrew Aplin for making available the ATR-FTIR mineral analysis data presented here. We express our gratitude to Ferdinand Perssen and Anika Zabel for their technical support. The China Scholarship Council is acknowledged for funding Yuanjia Han's Ph.D. scholarship.


## EDITOR'S NOTE

Color versions of all figures can be seen in the online version of this paper.

(source unit). Furthermore, molecular fractionation, i.e., a preferential expulsion of lower molecular weight hydrocarbons (*n*-alkanes) could be calculated.

An additional practical result for source rock assessment is that corrected S2 (petroleum generated by pyrolysis) and TOC values should be calculated by combining Rock-Eval pyrolysis data on whole rocks and rocks following Soxhlet extraction. Using parameters based on unextracted rock only, the expulsion of petroleum is systematically overestimated and the degree of kerogen conversion is, therefore, concomitantly underestimated.

## INTRODUCTION

The Barnett Shale is arguably the most well-known shale resource play in the United States. After the first Barnett well was drilled in 1981, a protracted development evolved over approximately 17 yr (Bowker, 2003). Initially, exploration targets were restricted to a core-gas-producing area (Figure 1). It was not until 2002, triggered by the application of both hydraulic stimulation and horizontal drilling techniques, that exploration and development expanded into a much larger area (Martineau, 2007) (Figure 1). More than 15 trillion cubic feet of gas have been produced from the Barnett Shale gas play (Nicot et al., 2014). In addition, up to 22 million bbl of oil have been produced from unconventional Barnett Shale combination plays (Figure 1) (Texas-RRC, 2015).

The Barnett Shale resource play has been defined as a self-contained source-reservoir petroleum system characterized by (1) excellent organic matter richness and thickness, (2) a high gas charge thanks to the sequential cracking of kerogen and oil, (3) a bulk mineralogical composition favoring brittleness, and (4) nanoporosity in the organic matter created by cracking and shrinkage (Jarvie et al., 2007). Shale gas sweet spots in the Barnett Shale occur where hydrocarbon liquids are no longer present, either because of elevated maturity (vitrinite reflectance Ro > 1.5%) or pressure cycling during the two periods of burial followed by uplift that characterize regions of the Fort Worth Basin (Hill et al., 2007b). With the retrenching of gas prices, there has generally been a switch to optimize the production of hydrocarbon liquids, in areas of enhanced shale thickness and oil window maturities, for example, in Montague and Cooke Counties on the north side of the basin (Figure 1) (EOG Resources, 2013).

Although the role played by maturity in controlling bulk GOR is established, as summarized above, the effects of retention on the chemical composition of retained fluids are not yet widely known, be that for the Barnett or unconventional resource plays in general. This has to be remedied because even subtle changes in bulk fluid

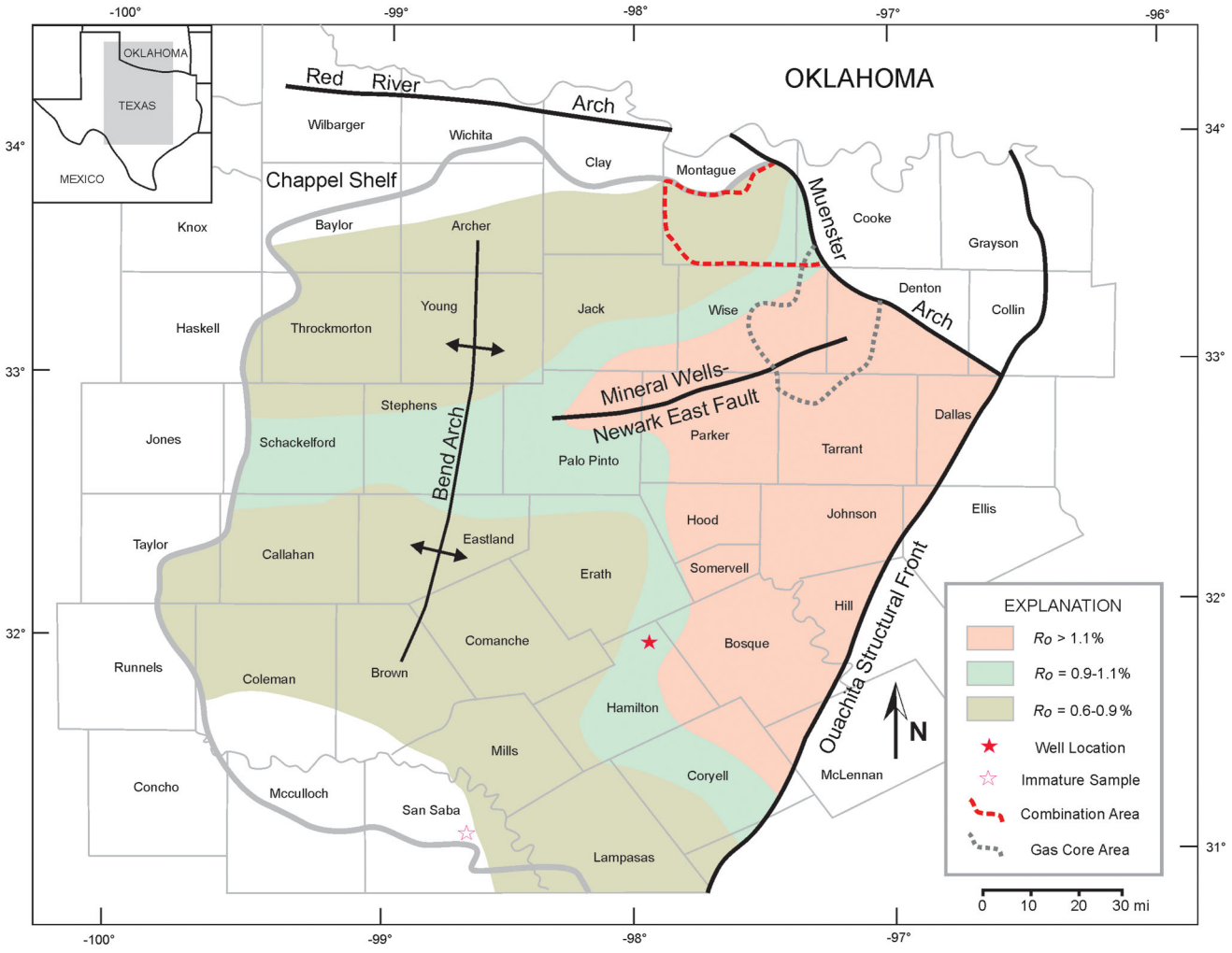


F1:1 **Figure 1.** Study location within the Fort Worth Basin. Basin structural elements are taken from Pollastro et al. (2007) and Hill et al. Q3 (2007).

composition are manifested by large differences in phase envelope geometry, with the result that pressure drawdown during production may or may not suit insitu fluid types. Furthermore, the sorptive properties of fluids on mineral and kerogen surfaces need to be taken into account in formulating production strategies. A compositional difference between source rock bitumen and petroleum in reservoirs was first observed by Brenneman and Smith (1958): although oil in reservoirs is enriched in saturated hydrocarbons, the bitumen extracted from shale is rather enriched with asphaltenes and resins (Tissot and Welte, 1984). This compositional difference is generally accepted to be a consequence of expulsion fractionation, i.e., as the fluid leaves the source environment. The preferential expulsion of aliphatic over aromatic hydrocarbons was first noted by Baker (1962). A preferential expulsion sequence (saturated hydrocarbons > aromatic hydrocarbons > polar compounds), i.e., chemical fractionation because of the polarity of compounds, was proposed by Leythaeuser et al. (1988a) at shale-sandstone contacts. This compositional sequence was then reproduced in the laboratory experiments of Lafargue et al. (1990) and Sandvik et al. (1992), and eventually theoretically modeled by Ritter (2003) and Kelemen et al. (2006). A preferential expulsion of smaller molecular size components over larger ones, i.e., physical fractionation, has also been documented as having taken place (Mackenzie et al., 1983; Leythaeuser et al., 1984), though the phenomenon is not always readily discernable (Leythaeuser et al., 1988c; Eseme et al., 2007). In unconventional shale

systems, such as the "tight" Barnett Shale, intraformational migration over centimeters within the source rock itself to isolated pores or structures might also bring about fractionation (Jarvie, 2014). Indeed, bitumens with differing chemical signatures, even at the submicrometer scale, have been reported for oil window maturity in Barnett Shale (Bernard et al., 2012; Bernard and Horsfield, 2014).

When considering fractionation, lithological facies play an important and underlying control, at different operating scales. In hybrid shale-oil systems (e.g., Bakken Shale or Niobrara shale-oil plays), continuous organic-rich and organic-lean intervals are juxtaposed. Production of oil is usually much more effective from the originally organic-lean lithofacies that is because of improved oil quality (migration fractionation ostensibly leads to the enhanced migration of smaller molecular size compounds with lower viscosity), added storage potential, and low sorption affinities (Jarvie, 2012). One goal of this paper is, therefore, to find potential sweet spots within the Marathon 1 Mesquite well Barnett Shale and correlate those with its "lithology," even though the Barnett is described as a "tight" shale-oil play and oil is usually produced from tight mudstones with some related matrix porosities (EOG Resources, 2010).

Mineral composition plays an important role in fracture stimulation of all shale resource plays (Bowker, 2007; Jarvie et al., 2007; Bunting and Breyer, 2012) as well as in reservoir diagenesis (Milliken et al., 2012). Within the Barnett Shale gas play, sedimentary intervals exhibiting prominent quartz contents play an important role for both fracture stimulation and oil retention. Most important, the primary producing facies of the Barnett Shale is composed of approximately 45 vol. % quartz (Bowker, 2003). Rather than detrital quartz, microcrystalline quartz is the major component of the siliceous Barnett facies (Loucks and Ruppel, 2007). Milliken et al. (2007) interpreted the microcrystalline quartz in Barnett Shale as being derived from mainly agglutinated foraminifera, whereas others have emphasized the importance of siliceous sponge spicules (Hickey and Henk, 2007; Slatt and O Brien, 2011; Abouelresh and Slatt, 2012).

In this paper, we (1) assess the amount and quality of retained hydrocarbons, (2) reveal the controls on hydrocarbon retention, including the role played by minerals, (3) decipher the primary migration process and related fractionation effects, (4) formulate a conceptual hydrocarbon generation-retention-expulsion model, and (5) calculate expulsion efficiency using compositional mass balance, including assessing the influence of retained bitumen on source rock assessment. The object under study was a core from the Marathon 1 Mesquite well of Hamilton County, Texas (Figure 1).

## SAMPLES

In the Marathon 1 Mesquite well (Hamilton County, Texas; Figure 1), the Mississippian Barnett Shale unconformably overlies the Ordovician Ellenburger group and is unconformably overlain by the Pennsylvanian Marble Falls Limestone (Figure 2). Because of the absence of the "Forestburg limestone" (also see Abouelresh and Slatt, 2012), the Barnett Shale sequence is not divided into upper and lower parts. In fact, the Mississippian section is not well defined because of a lack of diagnostic fossils. The lower "shale" part of the overlying Marble Falls Limestone is commonly used as a marker unit, but it is also commonly mistaken on well logs as the upper Barnett. Therefore, this unit is sometimes referred to by industry as the "false Barnett" (Pollastro et al., 2007).

A suite of 120 core samples (Figure 2) from the Barnett Shale core 53 m (175 ft thick) of the Marathon 1 Mesquite well was investigated. Samples were taken at approximately 20″ intervals to adequately take the heterogeneity of the section into account.

Prior to sampling, five intervals had been recognized based on the gamma-ray (GR) log, beginning with a high response at the Barnett Shale base that can be traced throughout most of the basin (Pollastro et al., 2007). Geochemical parameters were later used to complement and refine the definition of each interval. As previously stated and defined by Pollastro et al. (2007), the lower "shale" part of the Marble Falls Limestone is often mistaken as a part of the Barnett Shale ("false" Barnett) and is here called as the first interval (Figure 2). It is characterized by GR values less than 100 API. The second interval is defined by a high **Q4**

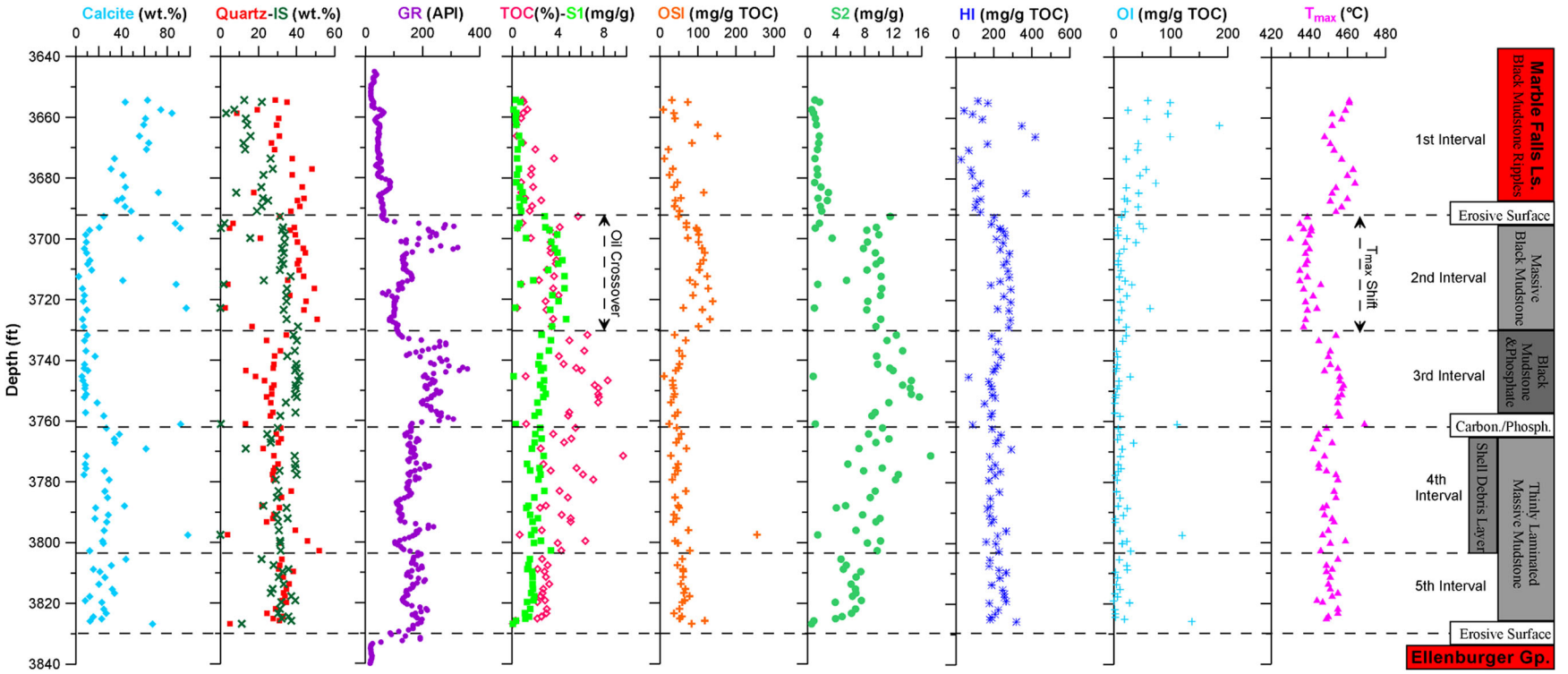


**Figure 2.** Geochemical depth profile of the Marathon 1 Mesquite well. Interval subdivisions are based on (1) gamma-ray (GR) log, (2) core description, (3) Rock-Eval parameter, and (4) attenuated total reflection Fourier transform infrared mineralogy. IS = illite and smectite; GR = gamma ray; TOC = total organic carbon; S1 = thermally extractable petroleum; OSI = oil saturation index (S1/TOC × 100); S2 = petroleum generated by pyrolysis; HI = hydrogen index (S2/TOC × 100); OI = oxygen index (S3/TOC × 100); $T_{max}$ = temperature at which S2 generation rate is maximum. F2:1 F2:2 F2:3 F2:4

GR response at the top (>200 API), which gradually decreases to values approximately 100 API. High GR responses between 200 and 350 API are observed throughout the third interval. The fourth interval is separated from the third interval by a sharp decrease in the GR response, most likely because of the lack of phosphate (Hickey and Henk, 2007). Throughout the fourth and fifth intervals, API values fluctuate between 100 and 200, and sedimentary aspects as well as organic matter richness were used to separate the two intervals, as described later. Strata within the fourth interval are characterized by the presence of shell debris layers (Figure 2). Below the fifth interval, i.e., below an erosive surface and within the Ellenburger Group, the GR response strongly diminishes to values approximately 25 API.

In addition to the Marathon 1 Mesquite well samples, one immature sample from a quarry in San Saba County, Texas, (Figure 1) was analyzed for mass balance calculations. It has a TOC content of 11.70% and a hydrocarbon index (HI = S2/TOC × 100) of 495 mg HC/g TOC. Its $T_{max}$ (temperature at maximum rate of petroleum generation by pyrolysis) value is 420°C (788°F), equivalent to 0.40% Rc (calculated vitrinite reflectance). The reader is referred to Bernard et al. (2012) and Romero-Sarmiento et al. (2014) for a detailed outline of the outcrop sample's geochemistry.

## ANALYTICAL METHODS

### Attenuated Total Reflection Fourier Transform Infrared Spectroscopy

Attenuated total reflection Fourier transform infrared (ATR-FTIR) spectroscopy was performed on 99 samples to semiquantitatively determine their bulk mineralogical compositions. This technique determines the bulk mineralogy in a quick, semiquantitative way within an 5% error margin for each mineralogical group, i.e., quartz, feldspars, total clay (illite-smectite [I-S], kaolinite, chlorite), and total carbonate (calcite, dolomite) (Adamu, 2012). Pyrite and apatite cannot be accounted for. The entire ATR-FTIR spectrum was baseline linearized by division of the highest peak intensity (Adamu, 2012).

### Thin Section and Scanning Electron Microscopy

Sample blocks were solvent extracted for 48 hr at 40°C (104°F) using a dichloromethane/methanol mixture (DCM/1%MeOH) and then mechanically polished both parallel (21 slices) and perpendicular (20 slices) to the lamina. Thin sections were first analyzed under transmitted white light, reflected white light, and blue light excitation to reveal organic-inorganic relationships. Scanning electron microscopy (SEM) was then conducted on 14 Au/Pd coated sections as well as on five rock fragments for further identification and characterization. Back-scattered electron and secondary electron images were taken with a 12.5 mm (0.49 in.) working distance. The X-ray stage mapping for Si, Mg, Ca, Al, Fe, and C was performed by energy dispersive spectroscopy using a 20 kV accelerating voltage.

### Rock-Eval Pyrolysis and Total Organic Carbon Content Determination

Rock-Eval pyrolysis (Espitalie et al., 1977) was performed on 99 whole-rock samples using a Rock-Eval 6 instrument. Seventeen solvent extracted samples were also investigated to evaluate the effects of retained hydrocarbons on Rock-Eval results. For total organic carbon (TOC) analysis, a Leco SC-632 combustion oven (1350°C [2462°F] in oxygen for oxidation) was used with infrared (IR) detection, after treating finely crushed rock samples with HCl (1:9 HCl:water) at 60 ± 5°C (140 ± 41°F) to remove carbonate.

### Thermovaporization/Open System Pyrolysis-Gas Chromatography

Thermovaporization and open-system pyrolysis gas chromatography (Tvap-GC and Py-GC) was carried out on 33 selected samples to sequentially characterize free hydrocarbons and labile kerogen, respectively, on a molecular level. Up to 35 mg of each, untreated and powdered whole rock samples were placed into glass capillaries (microscale sealed vessels), which were then sealed and introduced into a Quantum MSSV-2 Thermal Analyzer© (Horsfield

et al., 2015). Prior to each Tvap analysis, the tube was purged at 300°C (572°F) for 5 min to mobilize contaminants from the outside surface. It was then crushed by a piston device, releasing hydrocarbons from the tube to a liquid nitrogen cooled trap (−178°C [–352°F]). After 10 min, products were liberated (300°C [572°F]) and directly transferred into an Agilent GC 6890A gas chromatograph, as described by Keym et al. (2006). After the Tvap analysis was completed, the furnace was raised from 300° to 600°C (572° to 1112°F) at 50°C/min (122°F/min) and held for 2 min. Generated pyrolysis products were collected in the liquid-nitrogen-cooled trap and subsequently analyzed as described for Tvap.

For both methods, product quantification of different boiling ranges and individual compounds was based on external standardization using *n*-butane. Prominent hydrocarbon peaks were identified by reference chromatograms and using GC ChemStation© software from Agilent Technologies.

### Extraction and Fractionation

Between 10 and 100 g (0.35 and 4 oz) of roughly powdered shale material (17 samples, Table 1) was extracted for 48 hr at 60°C (140°F) in a Soxhlet apparatus (Soxhlet, 1879) using the ternary azeotropic solvent system (30:38:32 methanol:acetone:chloroform). After extraction, the extracts were subjected to asphaltene precipitation and medium pressure liquid chromatography (MPLC) fractionation.

Asphaltene precipitation was performed according to the linear and reproducible method developed by Theuerkorn et al. (2008). The MPLC was carried out using the method of Radke et al. (1980) to obtain aliphatic hydrocarbons, aromatic hydrocarbons, and hetero-(NSO) compounds from the maltenes fraction (17 samples). Prior to MPLC fractionation, 1-ethylpyrene was added as internal standard to quantify aromatic hydrocarbons in subsequent gas chromatography-mass spectrometry (GC-MS) analysis.

### Gas Chromatography-Mass Spectrometry

The aromatic fraction from MPLC fractionation was analyzed (17 samples, Table 2) using GC-MS. The GC-MS method has been described by Haberer et al. (2006), and uses an Agilent 6890A gas chromatograph coupled with a Finnigan MAT 95 XL MS in electron impact mode (70 eV) with a source temperature of 260°C (500°F). Full-scan mass spectra were recorded from m/z 50 to 650 Da at a scan rate of 1 scan per second and an internal scan delay of 0.2 s. The qualification and quantification of individual compounds were carried out using the software XCALIBUR.

## RESULTS

### Bulk Mineralogical Composition

The bulk mineralogical composition of the Barnett Shale sample set is shown in Figure 2, in which strong and systematic depth-dependent heterogeneities are revealed. Calcite (25%–85%) is the dominant mineral in the false Barnett (first interval), and clay mineral contents are generally less than 30%. Quartz becomes the dominant mineral (>40%) approaching the second interval, in which clay contents range between 30% and 40%. This interval can be described as siliceous, with carbonate contents less than 15%. Some carbonate-rich layers, or carbonate concretions, were nevertheless sampled and appear as outliers. The I-S mixed layer clay minerals dominate (>35%) the third interval, in which carbonate contents are also less than 15%. This interval can be described as argillaceous, as clay contents generally exceed quartz contents (10%–30%). Calcite, quartz, and I-S mixed-layer minerals are present in approximately equal proportions within the fourth and fifth intervals, i.e., quartz ranges between 25% and 45%, clay minerals range between 25% and 40%, and carbonates range between 10% and 40%.

Relative amounts of quartz, I-S mixed layer clay minerals, and calcite are shown in Figure 3. Most samples from the siliceous second interval, with the exception of carbonate concretions, clearly plot separately (stippled circle) from samples from the argillaceous third interval (solid circle). The majority of samples from the calcareous fourth and fifth intervals occupy an area in between that of samples from the carbonate-rich "false Barnett" and samples from the second and third interval.

**Table 1.** Rock-Eval Pyrolysis before and Subsequent to Soxhlet Extraction

| | | | Unextracted Rock | | | | | Extracted Rock | | | | | | |
|---|---|---|---|---|---|---|---|---|---|---|---|---|---|---|
| Sample | | Depth (ft) | S1 (mg/g) | S2 (mg/g) | $T_{max}$ (°C) | HI (mg/g TOC) | TOC (%) | S1* (mg/g) | S2* (mg/g) | $T_{max}$* (°C) | HI* (mg/g TOC) | TOC* (%) | $T_{max}$ Shift (°C) | Total Oil (mg/g) |
| G009583 | 1st | 3684.80 | 0.91 | 2.92 | 452 | 370 | 0.79 | 0.05 | 0.41 | 449 | 92 | 0.45 | −3 | 3.42 |
| G009584 | 1st | 3686.65 | 0.62 | 1.47 | 460 | 131 | 1.12 | 0.06 | 0.63 | 456 | 65 | 0.97 | −4 | 1.46 |
| G012611 | 2nd | 3710.26 | 2.91 | 7.23 | 436 | 216 | 3.34 | 0.09 | 3.55 | 444 | 132 | 2.68 | 8 | 6.59 |
| G009600 | 2nd | 3710.30 | 3.15 | 8.33 | 435 | 274 | 3.04 | 0.09 | 4.47 | 448 | 191 | 2.34 | 13 | 7.01 |
| G009601 | 2nd | 3712.40 | 4.55 | 10.3 | 439 | 281 | 3.66 | 0.13 | 4.59 | 453 | 174 | 2.63 | 14 | 10.26 |
| G009602 | 2nd | 3715.00 | 0.72 | 1.43 | 446 | 183 | 0.78 | 0.04 | 0.3 | 446 | 50 | 0.60 | 0 | 1.85 |
| G012612 | 2nd | 3720.59 | 3.28 | 7.2 | 439 | 232 | 3.11 | 0.11 | 3.29 | 451 | 138 | 2.39 | 12 | 7.19 |
| G012613 | 2nd | 3722.69 | 3.11 | 6.46 | 441 | 199 | 3.25 | 0.08 | 3.58 | 446 | 135 | 2.65 | 5 | 5.99 |
| G012616 | $3rd^U$ | 3731.66 | 3.24 | 12.74 | 450 | 200 | 6.38 | 0.14 | 9.31 | 453 | 163 | 5.71 | 3 | 6.67 |
| G009616 | $3rd^U$ | 3742.60 | 2.74 | 11.52 | 455 | 206 | 5.6 | 0.16 | 7.26 | 453 | 148 | 4.90 | −2 | 7.00 |
| G012617 | $3rd^L$ | 3745.49 | 2.53 | 11.51 | 458 | 173 | 6.67 | 0.12 | 8.57 | 456 | 140 | 6.12 | −2 | 5.47 |
| G009619 | $3rd^L$ | 3746.70 | 2.79 | 14.54 | 456 | 174 | 8.35 | 0.15 | 11.82 | 457 | 152 | 7.80 | 1 | 5.51 |
| G012618 | $3rd^L$ | 3746.80 | 2.46 | 15.88 | 455 | 183 | 8.69 | 0.17 | 13.13 | 456 | 161 | 8.17 | 1 | 5.21 |
| G009621 | $3rd^L$ | 3749.20 | 2.73 | 14.38 | 457 | 191 | 7.53 | 0.19 | 10.82 | 456 | 157 | 6.90 | −1 | 6.29 |
| G012622 | $4th^U$ | 3767.13 | 1.99 | 9.34 | 452 | 186 | 5.01 | 0.1 | 7.14 | 454 | 156 | 4.59 | 2 | 4.19 |
| G009647 | $4th^L$ | 3797.50 | 1.66 | 1.43 | 447 | 220 | 0.65 | 0.03 | 0.26 | 447 | 71 | 0.37 | 0 | 2.83 |
| G009650 | 5th | 3802.70 | 3.39 | 9.75 | 446 | 227 | 4.3 | 0.16 | 6.87 | 455 | 187 | 3.67 | 9 | 6.27 |

*= values for extracted samples; total oil = S1 + (S2–S2*); TOC* = TOC–total oil/10; HI* = [S2*/TOC*] × 100.

T2:1 **Table 2.** Total Extract and Bulk Chemical Fraction Yields*

| | | | | Fraction Yields | | | | | | | |
|---|---|---|---|---|---|---|---|---|---|---|---|
| T2:3 | | | | Ali. | Aro. | Res. | Asp. | Ali. | Aro. | Res. | Asp. | |
| T2:4 | Sample | | Depth (ft) | Concentration (mg/g) | | | | Composition (%) | | | | Extract Yield (mg/g) |
| T2:5 | G009583 | 1st | 3684.80 | 0.52 | 0.07 | 0.77 | 0.53 | 27.56 | 3.84 | 40.65 | 27.96 | 1.90 |
| T2:6 | G009584 | 1st | 3686.65 | 0.51 | 0.14 | 0.46 | 0.14 | 40.78 | 11.01 | 37.03 | 11.18 | 1.24 |
| T2:7 | G012611 | 2nd | 3710.26 | 4.26 | 0.95 | 1.45 | 0.17 | 62.45 | 13.88 | 21.20 | 2.48 | 6.82 |
| T2:8 | G009600 | 2nd | 3710.30 | 3.97 | 0.80 | 1.25 | 0.27 | 63.12 | 12.66 | 19.93 | 4.29 | 6.29 |
| T2:9 | G009601 | 2nd | 3712.40 | 5.05 | 1.16 | 1.97 | 0.27 | 59.79 | 13.77 | 23.29 | 3.15 | 8.45 |
| T2:10 | G009602 | 2nd | 3715.00 | 0.45 | 0.09 | 0.55 | 0.08 | 38.16 | 7.61 | 47.09 | 7.14 | 1.17 |
| T2:11 | G012612 | 2nd | 3720.59 | 4.23 | 1.10 | 1.16 | 0.24 | 62.76 | 16.37 | 17.24 | 3.62 | 6.74 |
| T2:12 | G012613 | 2nd | 3722.69 | 3.69 | 0.97 | 1.21 | 0.22 | 60.51 | 15.92 | 19.89 | 3.68 | 6.10 |
| T2:13 | G012616 | $3rd^U$ | 3731.66 | 2.89 | 0.98 | 1.46 | 0.29 | 51.36 | 17.49 | 26.00 | 5.15 | 5.62 |
| T2:14 | G009616 | $3rd^U$ | 3742.60 | 2.72 | 0.82 | 1.58 | 0.41 | 49.25 | 14.79 | 28.60 | 7.35 | 5.52 |
| T2:15 | G012617 | $3rd^L$ | 3745.49 | 1.77 | 0.78 | 0.97 | 0.27 | 46.69 | 20.63 | 25.49 | 7.18 | 3.79 |
| T2:16 | G009619 | $3rd^L$ | 3746.70 | 1.16 | 0.81 | 1.69 | 0.37 | 28.84 | 20.10 | 41.92 | 9.13 | 4.02 |
| T2:17 | G012618 | $3rd^L$ | 3746.80 | 1.96 | 0.93 | 1.48 | 0.23 | 42.58 | 20.21 | 32.18 | 5.04 | 4.61 |
| T2:18 | G009621 | $3rd^L$ | 3749.20 | 1.63 | 0.62 | 1.34 | 0.27 | 42.38 | 15.96 | 34.72 | 6.93 | 3.85 |
| T2:19 | G012622 | $4th^U$ | 3767.13 | 1.94 | 0.79 | 1.21 | 0.23 | 46.49 | 18.87 | 29.10 | 5.54 | 4.17 |
| T2:20 | G009647 | $4th^L$ | 3797.50 | 0.86 | 0.13 | 0.67 | 1.24 | 29.59 | 4.56 | 23.16 | 42.69 | 2.90 |
| T2:21 | G009650 | 5th | 3802.70 | 4.01 | 1.27 | 1.81 | 0.19 | 55.11 | 17.43 | 24.83 | 2.64 | 7.28 |

T2:22 *Ali. = aliphatic hydrocarbons; Aro. = aromatic hydrocarbons; Res. = resins (NSO-compounds); Asp. = asphaltenes.

The calcite content is plotted versus the content of I-S mixed layer clay minerals in Figure 4, and compared to published X-ray diffraction data (inset) (Jarvie et al., 2005; Milliken et al., 2012). A similar relationship is evident for all data sets, i.e., increasing clay mineral content with decreasing calcite content. Because mixed layer minerals (I-S) and calcite are thought to represent extrabasinal and intrabasinal input, respectively (Hickey and Henk, 2007; Loucks and Ruppel, 2007; Milliken et al., 2012), such a general negative correlation can be expected. Interestingly though, the ATR-FTIR results reveal the presence of two "parallel" groups, each having comparable slopes but offset *y*-intercepts. One group consists of samples from the entire sequence, i.e., samples from all intervals, which show a perfect negative correlation between calcite and I-S minerals. The second group also shows excellent correlation, but plots below the trend line of the first group and exhibits generally lower calcite contents, whereas clay contents are exclusively higher than 30%. Samples of this second group are mainly from the second interval that is, as discussed above, quartz dominated (Figure 3, stippled circle).

## Petrological Characteristics

Thin-section identification and SEM examination of Marathon 1 Mesquite samples show that quartz is present in the form of both extrabasinal grains (Figure 5A, M) and intrabasinal debris, i.e., sponge spicules (Figure 5A, M, N) and agglutinated foraminifera (Figure 5D–F). The latter are the main two kinds of biogenic quartz reported to occur in the Barnett Shale (Papazis and Milliken, 2005; Hickey and Henk, 2007; Loucks and Ruppel, 2007; Milliken et al., 2007, 2012; Slatt and O Brien, 2011; Abouelresh and Slatt, 2012).

The quartz in samples of the siliceous second interval (e.g., Figure 3) consists mainly of intrabasinal, biogenic sponge spicules (Figure 5A, M, N), and clay sized, presumably authigenic quartz disseminated in the matrix (Figure 5N). Milliken et al. (2012) reported that clay-sized microcrystalline

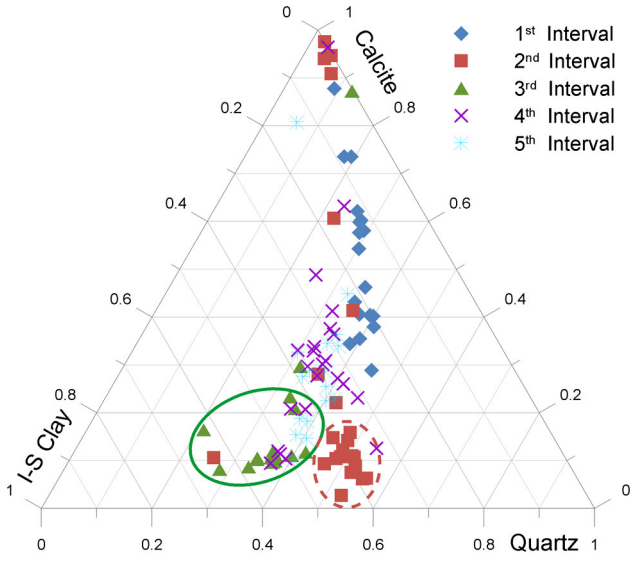


F3:1 **Figure 3.** Attenuated total reflection Fourier transform infra-
F3:2 red bulk mineralogical composition. The siliceous lithofacies
F3:3 (stippled circle) and argillaceous lithofacies (solid circle) can be
F3:4 distinguished.

414 quartz within the matrix is of similar origin than that
415 of silicified sponge spicules (same luminescence).
416 The interior chamber of sponge spicules contains
417 oil that fluoresces under blue light excitation
418 (Figure 5B) confirming the assertions of Slatt and
419 O Brien (2011) that the interior chamber of sponge
420 spicules might play an important role for the storage
421 of hydrocarbons. Quartz input in the form of aggluti-
422 nated foraminifera (Figure 5D–F) dominates
423 the third interval, and here, sponge spicules are rare.

It can be deduced that the biogenic quartz dominat- 424
ing the second interval, which appears as a distinct 425
mineralogical group in Figure 4, is indicative of a 426
different depositional pattern. The input of addi- 427
tional biogenic quartz dilutes the relationship 428
between extrabasinal I-S minerals and intrabasinal 429
calcite explaining the offset to lower values 430
(Figure 4). The presence of agglutinated foraminif- 431
era in the third interval offers only very limited bio- 432
genic quartz input to the sedimentary influx 433
because, according to Schieber et al. (2000) and 434
Milliken et al. (2007), agglutination is the earliest 435
form of foraminiferal cyst construction, which 436
means that the foraminifera cyst is achieved by 437
aggregating much of the detrital quartz. Although 438
foraminifera are biogenic, the quartz is mainly of 439
detrital origin (thus, neither opaline nor readily 440
recrystallized). Thus, samples from the third interval 441
do not exhibit a different mineralogical pattern in 442
Figure 4. 443

Clay minerals are interpreted as clay-sized detri- 444
tal particles under the optical microscope, but authi- 445
genic clay minerals can be observed in the chamber 446
of sponge spicules in the SEM (Figure 5C). Calcite 447
is the primary carbonate mineral (Figure 5N). 448
Calcite-dominated skeletal fragments are common, 449
especially in the fourth interval (Figure 5G). 450

Progressive burial and diagenesis, including 451
mechanical and chemical modifications, have signifi- 452
cantly modified the original sedimentary signature. 453

F4:1 **Figure 4.** Attenuated total
F4:2 reflection Fourier transform
F4:3 infrared illite-smectite (I-S)
F4:4 mixed layer clays versus calcite
F4:5 content. The X-ray diffraction
F4:6 data of the inset graph are taken
F4:7 from Jarvie et al. (2005) (calcite
F4:8 versus clay) and Milliken et al.
F4:9 (2012) (calcite versus I-S).

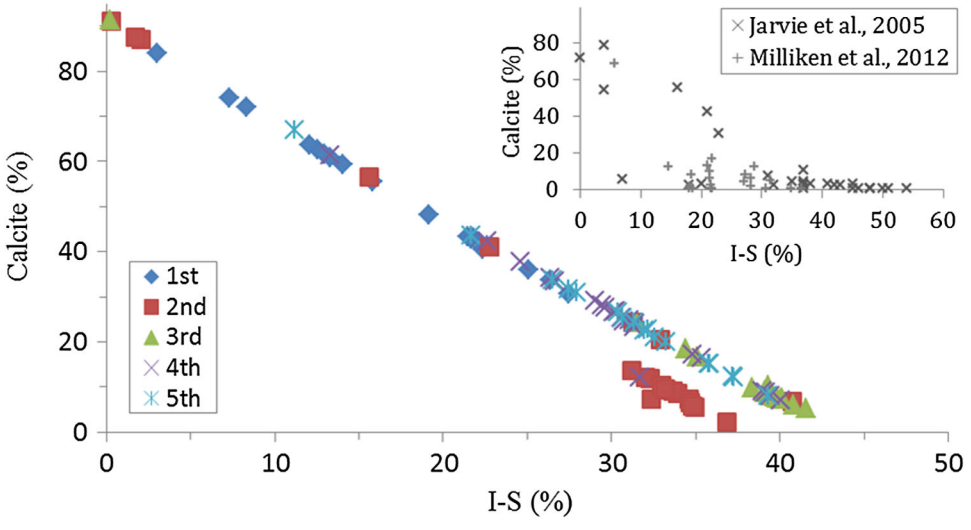

Calcite particles were locally dolomitized and replaced by silt-sized dolomite rhombs (Figure 5M). Chalcedonic fossil skeletons are found in its recrystallized form as single quartz crystals, and some are elongated parallel to the bedding, i.e., collapsed agglutinated foraminifera (Figure 5D–F). Papazis and Milliken (2005) and Milliken et al. (2007) interpreted microcrystalline quartz in the Barnett Shale as agglutinate foraminifera that have collapsed dramatically during compaction.

## Lithofacies

Loucks and Ruppel (2007) recognized for the Barnett shale three general lithofacies, i.e., laminated siliceous mudstone, laminated argillaceous lime mudstone (marl), and skeletal argillaceous lime packstone, in the central and north part of the Fort Worth Basin. In the east-central basin, Bunting and Breyer (2012) and Abouelresh and Slatt (2011) subdivided the laminated siliceous mudstone, into five and six lithofacies, respectively: (1) siliceous, noncalcareous mudstone; (2) siliceous, calcareous mudstone; (3) phosphatic deposit; (4) dolomitic mudstone; (5) calcite-rich, laminated deposit (bottom current deposit); (6) resedimented, spiculitic mudstone, etc. (Abouelresh and Slatt, 2012).

Most of the above-listed lithofacies can be roughly identified within the Marathon 1 Mesquite well, based on macroscale observations and mineralogic-petrologic investigations. The first interval is part of the Marble Falls Limestone and can therefore not be correlated with any of the above facies. It appears as a well-bedded mudstone with current ripples developed within the core, whereas carbonate is the dominant mineral.

The siliceous second interval appears mainly as a thinly laminated to massive black mudstone in the core. Based on bulk mineralogy, this correlates with the siliceous noncalcareous mudstone facies (Singh, 2008; Abouelresh and Slatt, 2012), which is ascribed to a low-energy, anaerobic depositional environment dominated by suspension settling. Nevertheless, zones of laminated to cross-laminated silty-shaly mudstones are also abundant, which correspond to the silty-shaly (wavy) interlaminated deposits described in Singh (2008). Consistent with the observed high contents of sponge spicules in this interval (Figure 5A–C, M, N), silt-sized grains within this facies are said to be mainly of sponge spicule origin (Abouelresh and Slatt, 2012).

The most organic-rich, argillaceous third interval appears in the core mainly as a thinly laminated to massive black mudstone corresponding to the siliceous noncalcareous mudstone facies described in Singh (2008) and Abouelresh and Slatt (2012). Thin, black phosphatic laminae also occur in alternation with thinly laminated black mudstone, and phosphatic nodules occur in pack to grainstone layers as hardgrounds. Both lithofacies are consistent with deposition in distal, starved basins, characterized by suspension settling processes and very low energy. The lack of sedimentary structures indicates that deposition in an euxinic environment (below the oxygen minimum layer) prevailed, explaining high organic matter and clay mineral contents in the third interval. High GR log responses are also prevalent. Because sponges do not inhabit euxinic conditions, they are rarely present, whereas agglutinated foraminifera, which are highly tolerant of conditions of low oxygenation (Bernhard, 1989; Gooday, 1994; Milliken et al., 2007), are the most abundant form of quartz (Figure 5D–F).

The carbonate-rich fourth and fifth intervals appear in the core mainly as laminated to massive mudstone, which is, especially in the fourth interval, often associated with shell debris layers (Figure 5G). Taking into account the bulk mineralogy, this correlates mainly with the calcareous facies (Singh, 2008; Abouelresh and Slatt, 2012), but the presence of siliceous noncalcareous mudstone facies in association with reworked shell deposits or calcareous lamina cannot be ruled out. The macroscopic heterogeneity within the fourth interval might be interpreted because of alternating quiet and high-energy periods. Sand-sized shell debris dominates over mud-sized clays (Figure 5G). Thus, the deposition under alternating oxic and anoxic conditions is reasonable. The siliceous calcareous mudstone facies dominates within the fifth interval. The calcareous content of this facies can be attributed to relatively shallower water, oxic conditions (Abouelresh and Slatt, 2012).

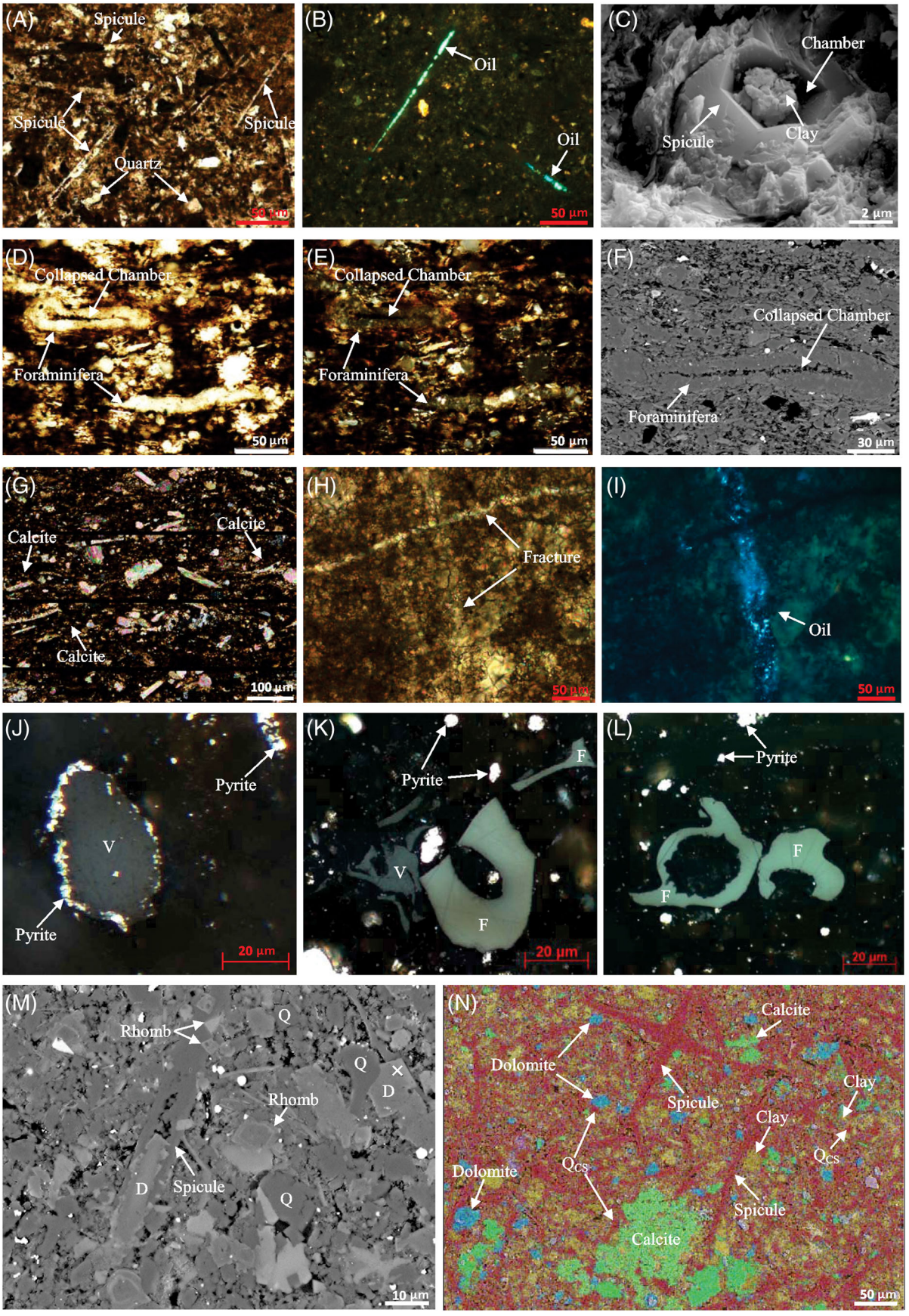
(A)
Spicule
Spicule
Spicule
Quartz
50 µm
(B)
Oil
Oil
50 µm
(C)
Chamber
Clay
Spicule
2 µm
(D)
Collapsed Chamber
Foraminifera
50 µm
(E)
Collapsed Chamber
Foraminifera
50 µm
(F)
Collapsed Chamber
Foraminifera
30 µm
(G)
Calcite
Calcite
Calcite
100 µm
(H)
Fracture
50 µm
(I)
Oil
50 µm
(J)
Pyrite
V
Pyrite
20 µm
(K)
Pyrite
F
V
F
20 µm
(L)
Pyrite
F
F
20 µm
(M)
Rhomb
Q
Q
X
D
Rhomb
D
Spicule
Q
10 µm
(N)
Calcite
Dolomite
Spicule
Clay
Clay
Qcs
Qcs
Dolomite
Spicule
Calcite
50 µm

## Organic Matter Characteristics

Although TOC can be as high as 20 wt. % in organic-rich facies (Bowker, 2003), the TOC content of the Barnett Shale averages 4.5 wt. % in the maturity range from 0.6% to 1.6% Ro (Jarvie et al., 2001a). The Barnett Shale samples from the Marathon 1 Mesquite well fit into this general scheme and exhibit an average TOC content of approximately 4% (Figure 2). The false Barnett Shale, i.e., first interval, and the fifth interval are relatively lean intervals, with average TOC values less than 3%. In the second to fourth intervals, TOC contents generally exceed 3%. The lower part of the third interval is richest in organic matter (TOC > 6%) and possesses highest hydrocarbon generative potentials (S2 > 12 mg/g). It is the best source rock of the succession and therefore here referred to as the major source unit.

The maturity of kerogen can be assessed by its pyrolysis-determined $T_{max}$ (Tissot and Welte, 1984; Peters, 1986) though the parameter is highly dependent on organic matter type (Horsfield et al., 1983). Applying the equation $R_c = 0.0180 \times T_{max} - 7.16$ proposed by Jarvie et al. (2001a) for the Barnett, the calculated average $R_c$ value of Marathon 1 Mesquite well samples is 0.94%. However, $T_{max}$ values are not similar throughout the vertical profile and fluctuate approximately 450°C (842°F) in a systematic way related to the aforementioned zonation of facies and mineralogy (Figure 2). For example, $T_{max}$ values of samples from the second interval show much lower values (~440°C [824°F], 0.76% $R_c$) than samples from the organic-matter-rich third interval (~455°C [851°F], 1.03% $R_c$). Low $T_{max}$ values can be caused by the presence of heavy bitumen (Kruge, 1983), and this is confirmed by a shift to higher values (~450°C [842°F], 0.94% Ro) after Soxhlet extraction. In contrast, differences for samples from the third interval are small (Table 1). After extraction, $T_{max}$ values clearly shift to higher values (445–455°C [833–851°F]), peaks of thermally extractable petroleum (S1) are strongly diminished (as expected), and the area below the S2 curve is significantly decreased for samples of the second interval (Figure 6A). In the lower part of the third interval and the upper part of the fourth interval, Rock-Eval traces before and after extraction are qualitatively similar (similar $T_{max}$), except that minor S2 "preshoulders" are removed (Figure 6B).

**Figure 5.** Photomicrographs showing petrographic features. (A) Sample G009601 from the second interval, depth 1132 m (3712.40 ft), parallel to bedding, under polarized light; siliceous sponge spicules and detrital quartz grains. (B) Sample G012606 from the second interval, depth 1128 m (3701.48 ft), parallel to bedding, under blue light excitation; fluorescent light, the interior chamber of sponge spicules are occupied by oil. (C) Sample G009600 from the second interval, depth 1131 m (3710.30 ft), coated core chips, perpendicular to bedding, secondary electron (SE) image; clay minerals within hollow chamber of siliceous sponge spicule. (D/E) Sample G012618 from the third interval, depth 1142 m (3746.80 ft), perpendicular to bedding, under polarized (D) and cross-polarized (E) light; siliceous agglutinated foraminifera elongated parallel to bedding, the compacted foraminifera test possesses a distinctive medial line indicative of the collapsed chamber. The mottled test grains under cross-polarized light are said to be of detrital origin. (F) Sample G012620 from the third interval, depth 1144 m (3754.08 ft), perpendicular to bedding, Back-scattered electron (BSE) image; siliceous agglutinated foraminifera. (G) Sample G012621 from the fourth interval, depth 1147 m (3764.29 ft), perpendicular to bedding, under cross-polarized light; calcite skeletal fragments. (H/I) Sample G009602 from the second interval, depth 1132 m (3715.00 ft); parallel to bedding under (H) cross-polarized and (I) fluorescent lights; two calcite cemented fractures. One fracture comprises cluster of oil inclusions. (J) Sample G012605 from the first interval, depth 1124 m (3686.66 ft), perpendicular to bedding, under reflected white light in oil immersion; vitrinite (V) and pyrite. The pyrite encircling vitrinite indicates reworking of organic matter by sulfur bacteria. (K) Sample G012617 from the third interval, depth 1141 m (3745.49 ft), parallel to bedding, under reflected white light in oil immersion; fusinite [F] and vitrinite [V]. (L) Sample G012624 from the fourth interval, depth 1155 m (3790.87 ft), perpendicular to bedding, under reflected white light in oil immersion; fusinite [F] and pyrite. (M) Sample G012611 from the second interval, depth 1131 m (3710.26 ft), parallel to bedding, BSE image; ferroan dolomite rhomb (the scanning electron microscope [SEM] composition of the area marked by a white cross: $CO_2$-20.16, MgO-14.04, $Al_2O_3$-1.68, $SiO_2$-19.56, $SO_3$-0.65, $K_2O$-0.25, CaO-31.01, $TiO_2$-0.11, $Fe_2O_3$-12.53, unit %), intrabasinal siliceous sponge spiclues and extrabasinal quartz grains (Q) can be identified. (N) Sample G012614 from the second interval, depth 1135 m (3723.46 ft), parallel to bedding, SEM-energy dispersive spectroscopy element mapping; quartz (siliceous sponge spicules and clay-sized quartz: Qcs) in red is the dominant mineral, clay (yellow) is finely dispersed, dolomites (blue) are scarce, and calcite (green) is the dominant carbonate.

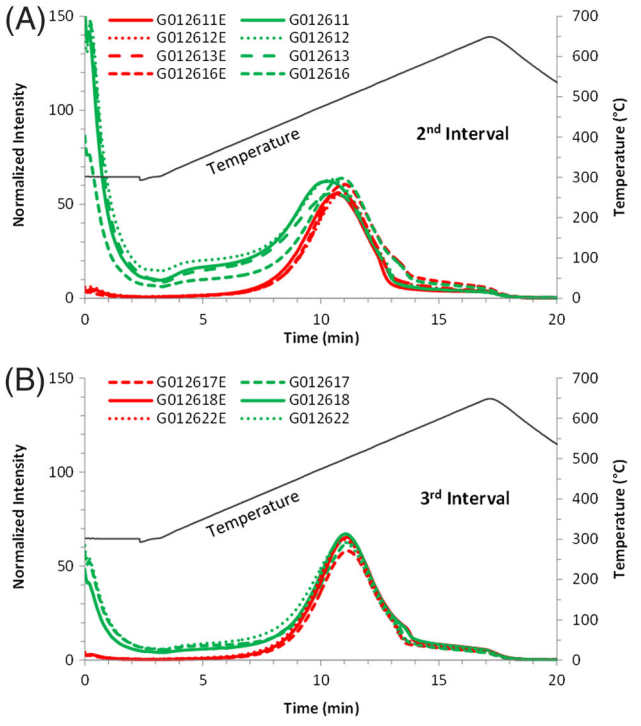


F6:1 **Figure 6.** Rock-Eval traces before and after Soxhlet extraction
F6:2 as a function of time, the extracted samples are marked with
F6:3 an "E" at the end of their sample number. Left *y*-axis is normal-
F6:4 ized by dividing the initial signal intensity with the sample weight
F6:5 and total organic carbon. Right *y*-axis indicates the temperature
F6:6 program. (A) Typical traces for samples from the second inter-
F6:7 val. (B) Typical traces for samples from the third interval (and
F6:8 the upper part of fourth interval).

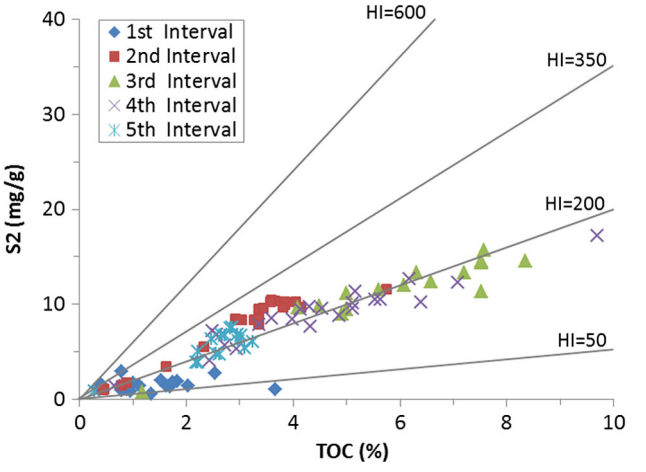


**Figure 7.** S2 versus total organic carbon lines of similar hydro- F7:1
gen index values are indicated. F7:2

595 In the Marathon 1 Mesquite well, most samples
596 fall along a 200 mg HC/g TOC hydrogen index trend
597 line in the S2 versus TOC content plot (Figure 7) of
598 Langford and Blanc-Valleron (1990). This represents
599 the remaining petroleum potential of a type II kero-
600 gen at late oil window maturity. Samples from the
601 false Barnett (first interval) exhibit average values of
602 only 100 mg HC/g TOC. The HI values in the second
603 interval are slightly enhanced (average ~250 mg HC/
604 g TOC). As described later, this likely represents the
605 contribution of nonvolatile petroleum or bitumen to
606 the S2 peak and is also responsible for the aforemen-
607 tioned shift in $T_{max}$ to lower values after extraction.
608 Likewise, S2 values also show a systematic decrease
609 after solvent extraction (Table 1 and Figure 8A). It
610 can be concluded from Figure 8A that HI values of
611 unextracted samples of all intervals represent a sys-
612 tematic overestimation (>14%) of the remaining
613 generation potential because of a portion of the
614 retained petroleum eluting in S2. The relevance of
615 such a process was already demonstrated by Barker
616 (1974) and Clementz (1979). After extraction, S2 val-
617 ues are approximately 50% lower for samples from
618 the second interval, whereas they are only approxi-
619 mately 25% lower for samples from the third to fifth
620 interval.

621 Concerning kerogen structure, the relative
622 amounts of (1) $C_{1-5}$ total hydrocarbons, (2) sum
623 of $C_{6-14}$ *n*-alk-1-enes and *n*-alkanes, and (3) sum
624 of $C_{15+}$ *n*-alk-1-enes and *n*-alkanes in pyrolysis
625 products fall near the boundary of the Gas &
626 Condensate and Paraffinic-Naphthenic-Aromatic
627 (P-N-A) Low Wax Petroleum Type Organofacies of
628 (Horsfield, 1989) (Figure 9A). The pyrolysate of
629 the immature sample from the San Saba outcrop
630 (cf. Romero-Sarmiento et al., 2014) is located within
631 the area of the P-N-A Low Wax facies, but it is
632 nevertheless very similar to the pyrolysate of more
633 mature samples from the Marathon 1 Mesquite well,
634 in that the alkyl chains in the kerogen are anoma-
635 lously short; this has already been documented for
636 the Bakken Shale in North Dakota of American and
637 Alum Shale in Sweden and Norway (Horsfield et al.,
638 1992; Muscio et al., 1994).

639 Kerogen type was further confirmed using sulfur
640 content and relative aromaticity from Py-GC data
641 (Figure 9B; Eglinton et al., 1990). The immature
642 Barnett Shale sample (filled circle) contains more

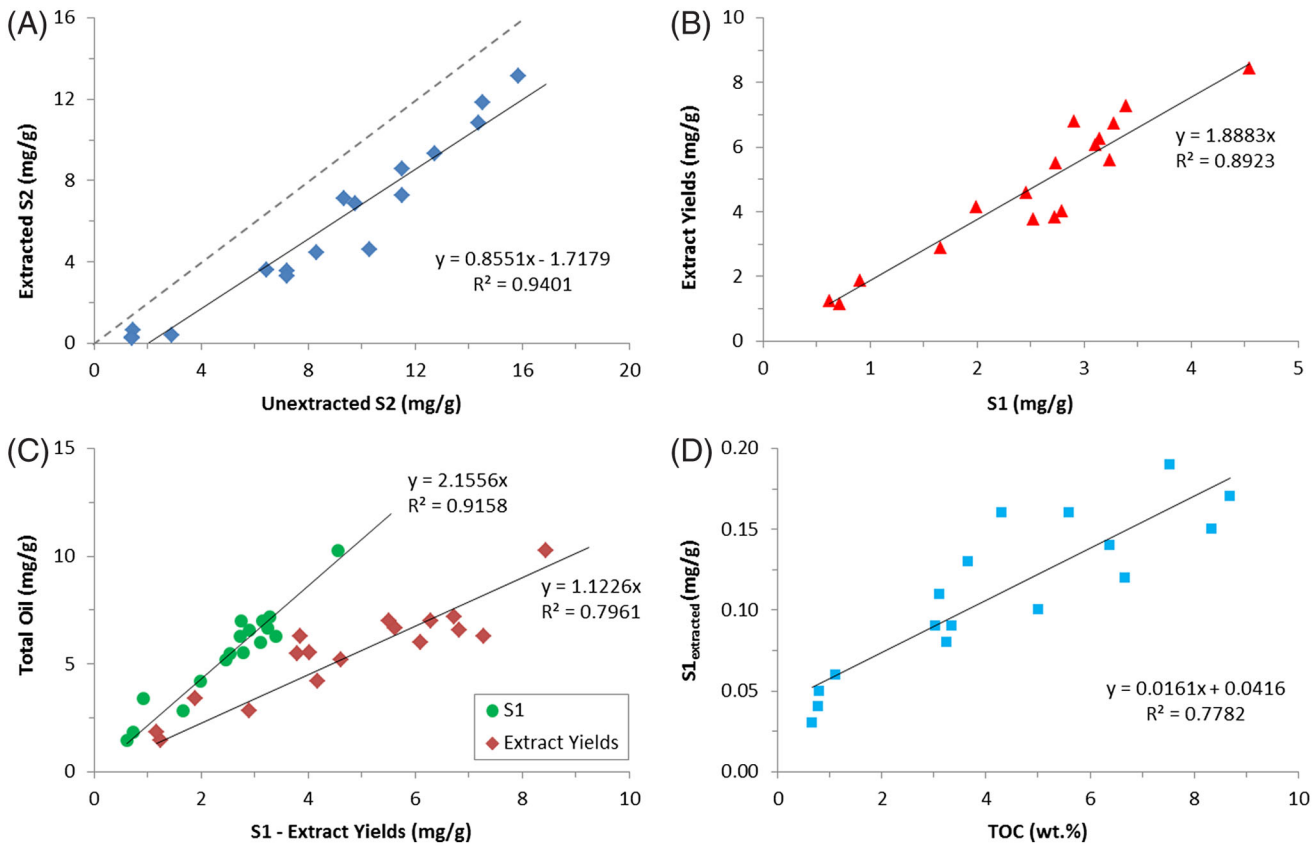


F8:1 **Figure 8.** Relationships between Rock-Eval proxies before and after solvent extraction and extract yields. (A) S2 values of unextracted
F8:2 versus extracted samples. (B) S1 values of unextracted samples versus extract yields. (C) S1 values of unextracted samples and extract
F8:3 yields versus calculated total oil (total oil = $S1_{wholerock}$ + $S2_{wholerock}$ − $S2_{extracted\ rock}$). (D) S1 of solvent extracted samples versus total
F8:4 organic carbon.

643 sulfur-bearing precursor structures (see Figure 9B)
644 than the more mature samples. This is no surprise
645 because many organic sulfur bonds are known to
646 crack at lower bond energies or "early" in the thermal
647 maturation process (Pepper and Corvi, 1995; Di
648 Primio and Horsfield, 1996).

## 649 Quantification of Retained Petroleum

650 The amount of retained, or stored, petroleum can be
651 inferred simply using Rock-Eval S1 values (Peters,
652 1986). Petroleum yields (S1) are shown for the entire
653 Marathon 1 Mesquite well in Figure 2. The false
654 Barnett Shale is a relatively organic-lean interval with
655 average S1 values less than 1 mg HC/g rock. S1 val-
656 ues generally decrease from 2.5 to 1.5 mg HC/g rock
657 because TOC decreases going from the third to the
658 fifth interval. In these intervals, organic matter con-
659 tent seems to be the controlling factor for the
660 retention of hydrocarbons. S1 values are highest in
661 the second interval (>3 mg HC/g Rock), thereby
662 exceeding values in the more organic-rich third and
663 fourth intervals. S1 values encountered for samples
664 from the second interval exceed TOC contents nomi-
665 nally, a feature called "oil crossover," and corre-
666 sponding to oil saturation index (OSI = [S1/TOC] ×
667 100) values higher than 100 mg HC/g TOC (Jarvie,
668 2012); values greater than 100 mg HC/g TOC indi-
669 cate an oil-saturated zone in which potentially pro-
670 ducible oil is present, producible because the "free"
671 oil can overcome a sorption threshold exerted by the
672 residual organic matter. Of course, measured S1
673 values represent a "minimum" for all samples (e.g.,
674 Jarvie and Baker, 1984) because light hydrocarbons
675 are lost during core retrieval, storage, and sample
676 preparation. It is thus conceivable that producible oil
677 may be found when values are less than 100 mg/g
678 TOC. In the present case of the Marathon 1

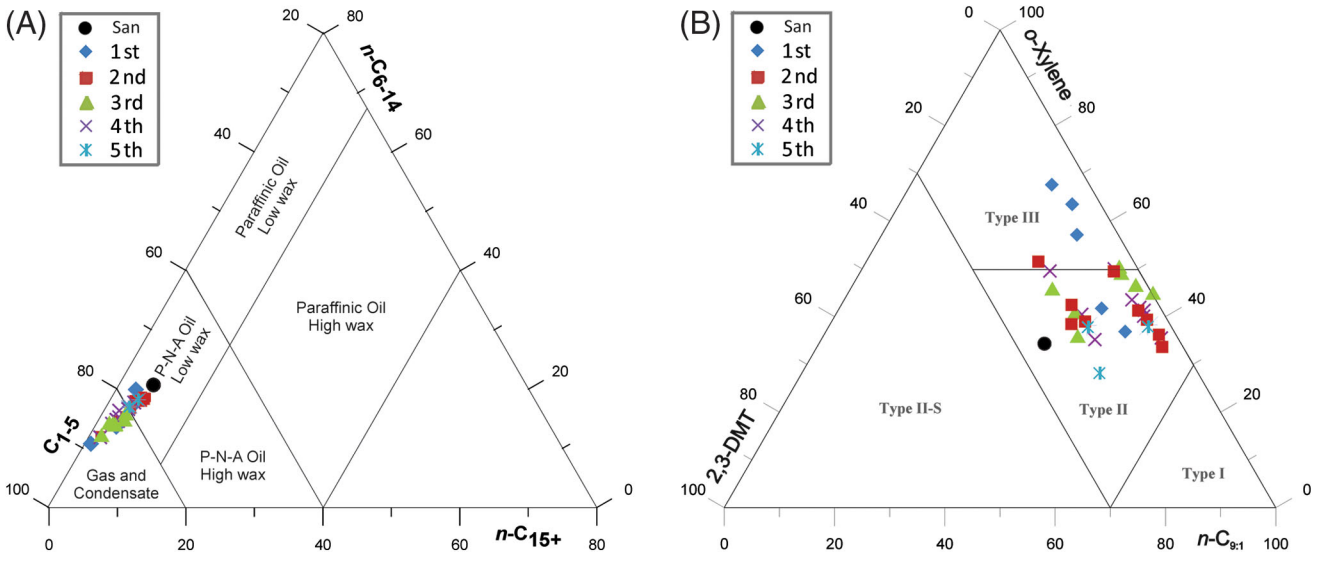


F9:1 **Figure 9.** Petroleum type organofacies definition after (A) Horsfield (1989) and (B) Eglinton et al. (1990). $C_{1-5}$ = total $C_{1-5}$ resolved
F9:2 pyrolysate; *n*-$C_{6-14}$ = $C_{6-14}$ *n*-alk-1-enes plus *n*-alkanes; *n*-$C_{15+}$ = $C_{15+}$ *n*-alk-1-enes plus *n*-alkanes; 2,3-DMT = 2,3-dimethylthiophene;
F9:3 *o*-xylene = ortho-xylene; *n*-$C_{9:1}$ = nonene.

Mesquite well, "oil crossovers" indicate that an interval exists in the Barnett Shale in which more hydrocarbons are stored or retained than in other intervals and this can be considered a sweet spot.

The amount of retained petroleum or bitumen can also be evaluated by the solvent extract yield (Claypool and Reed, 1976). Extract yields are less than 2 mg HC/g rock in the first interval, whereas they exceed 6 mg HC/g rock in the second interval (Table 2). Proceeding from the third to the fifth interval, extract yields generally decrease from 5 to 3 mg HC/g rock. This overall trend is very similar to the trend observed for the S1 values. In agreement with results of Claypool and Reed (1976), a good correlation exists between extract yields and S1 (Figure 8B), whereas the extract yields are systematically higher (1.9 fold) than the S1 values of unextracted samples. This suggests a strong signal coming from petroleum in all intervals and to a systematic underestimation of the total oil content in the vertical profile using only pyrolysis. S1 usually represents free organic compounds from $C_1$ to about $C_{32}$ (Peters, 1986) and has been verified by Tvap analysis (Horsfield et al., 2015), although Jarvie et al. (2001b) have documented the presence of $C_{50+}$ paraffin in thermal extraction using high-temperature GC. Nevertheless, $C_{17+}$ compounds may also be carried over into S2 by adsorption on rock matrix, followed by cracking (preshoulder areas in Figure 6) (Barker, 1974; Clementz, 1979; Dembicki et al., 1983).

The equation (Jarvie, 2012): Total oil = $S1_{wholerock} - S1_{extractedrock} + S2_{wholerock} - S2_{extracted\ rock}$ has been used to quantify the total retained petroleum (minus evaporative gas loss) because hydrocarbons below $C_{15-}$ are generally lost during solvent evaporation (Jarvie and Baker, 1984; Peters, 1986). Our result shows that the S1 peak of the extracted rock material (<0.2 mg HC/g sample) mainly consists of extraction solvents. The magnitude of this solvent contamination increases as organic matter content increases (Figure 8D), further indicative of the sorptive capacity of organic matter. Therefore and as a practical consequence, at least for our sample set, the S1 value of extracted samples was not subtracted as proposed by Jarvie (2012), because the amount of total oil would have been be underestimated, although only slightly. We modified the equation to Total oil = $S1_{wholerock} + S2_{wholerock} - S2_{extracted\ rock}$. Calculated total oil values of investigated samples are listed in Table 1 and shown in Figure 8C in comparison with thermal (S1) and solvent extract yields. Good correlations exist between calculated total oil (minimum amounts) with both the measured S1 and solvent extract yields, whereas solvent extract yields seem to be more approximate to the total amount of retained oil. Calculated total oil yields are only 1.1 fold higher than solvent extract yields whereas

they are 2.2 fold higher than S1 yields. Nevertheless, S1 can still be used conveniently as a screening tool for the general assessment of "free" oil content because its amount has been systematically underestimated by an average of approximately 54% in each interval.

## Composition of Retained Hydrocarbons

In the second interval, the relative amount of aliphatic hydrocarbons is much higher than in the third interval (Figure 10: 62% second versus 44% third). Vice versa, the bitumen of the third interval is relatively enriched in aromatic hydrocarbons (15% second versus 18% third) and especially polar compounds (23% second versus 38% third). Similarly, resins (20% second versus 31% third) and asphaltenes (3% second versus 7% third) are relatively enriched in the third interval. On a mg/g rock basis, approximately similar extraction yields of aromatic and NSO-compounds are observed in both intervals, whereas aliphatic compound yields are roughly twice as high in the second interval compared to the third interval (Table 2). Comparing these results to data published in Leythaeuser et al. (1988c) and the experimental data of Sandvik et al. (1992), fluids in the siliceous second interval are similar to expelled or reservoir petroleum, whereas fluids in the argillaceous third interval are similar to source rock extracts.

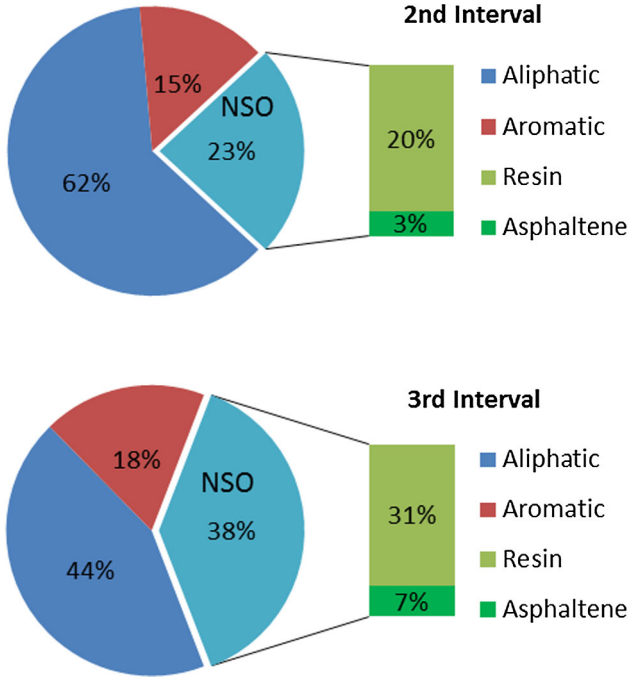


**Figure 10.** Average gross chemical composition of extracts from the second and third intervals.

The *n*-alkane distributions derived from thermal extraction (Tvap-GC) are presented as histograms in Figure 11. $C_1$ to $C_5$ gas components are depleted mainly because of selective loss because of evaporation during sample storage and handling (Larter, 1988; Sandvik et al., 1992). Short-chain *n*-alkanes ($C_{5-10}$) dominate thermal extracts of samples from the most organic-rich lower part of the third interval plus the upper part of fourth interval. The main carbon number gradually increases from *n*-$C_8$ in the third interval to *n*-$C_{13}$ in the second interval. A similar trend is also observed downward to the underlying intervals. Long-chain *n*-alkanes (*n*-$C_{17+}$) are depleted in the argillaceous third interval, whereas they are relatively enriched in the second interval (Figure 11). These differences are clearly shown in a ternary diagram (Figure 12), in which *n*-$C_{1-10}$, *n*-$C_{11-16}$, and *n*-$C_{17+}$ are used as coordinates. Samples of the second interval, reported earlier to be enriched in biogenic quartz (stippled circle, see Figure 3), are those enriched slightly in long-chain *n*-alkanes (Figure 12). In contrast, thermal extracts of the third interval (solid circle), dominated by clay (see Figure 3), are enriched in short-chain *n*-alkanes. For calcite-dominated samples, irrespective of which interval they belong to, a different compositional trend can be observed (Figure 12). The richer in carbonate a sample is, the higher is the proportion of long-chain *n*-alkanes. It can be deduced that different compositions of retained petroleum are associated with different lithological patterns.

Concentrations of pristane, phytane, *n*-$C_{17}$, and *n*-$C_{18}$ possess a similar vertical profile throughout the Marathon 1 Mesquite well (Figure 13A) in that they are depleted in most intervals whereas they are enriched in the siliceous oil crossover interval (second interval). The ratio of pristane to phytane (Pr/Ph) is a widely used biomarker index to assess the depositional environment and kerogen type (Brooks et al., 1969; Powell and McKirdy, 1973; Didyk et al., 1978; Powell et al., 1988; Peters et al., 1999; Arfaoui and Montacer, 2007;

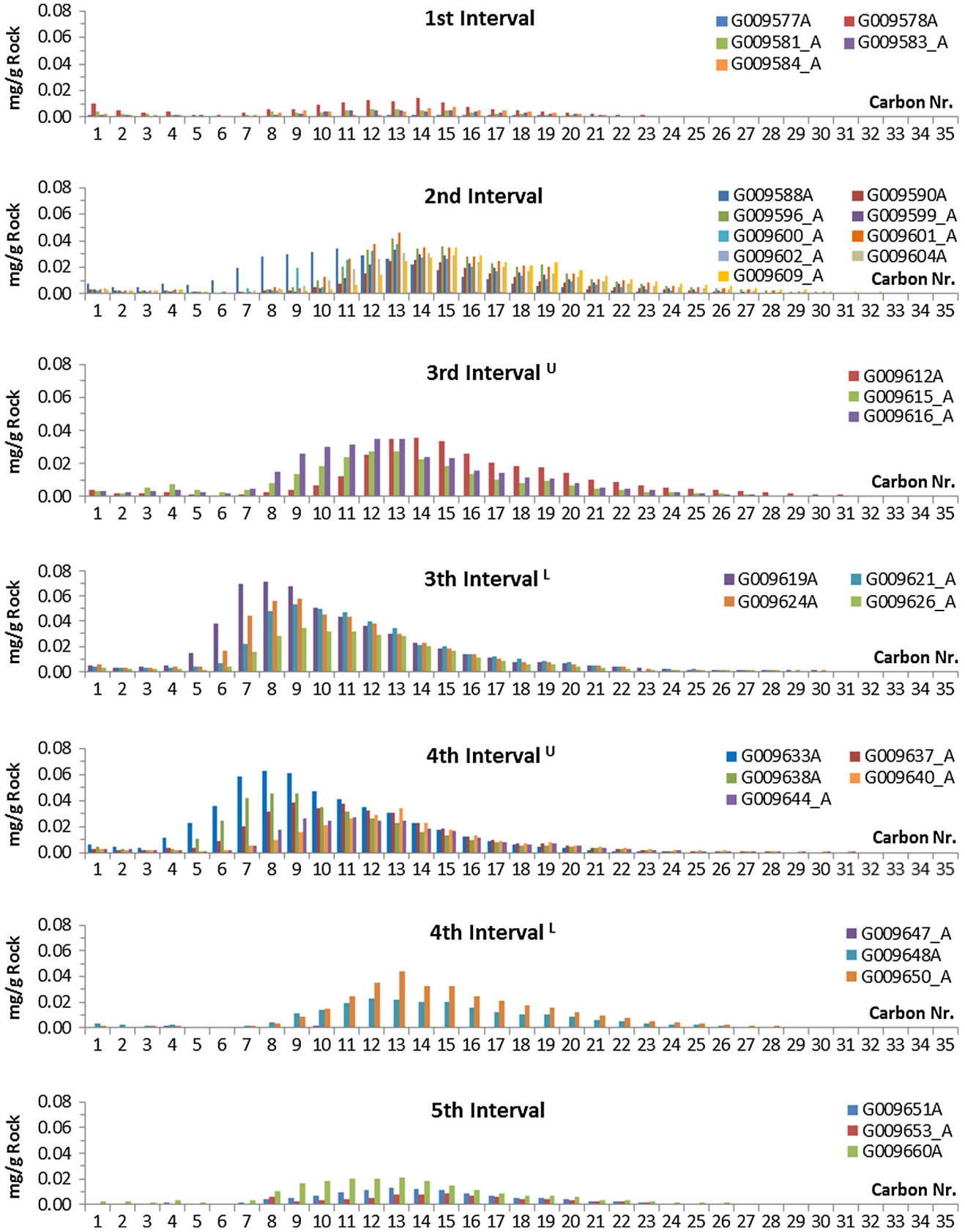


F11:1 **Figure 11.** Tvap-gas chromatography *n*-alkane distribution for samples from all intervals. Numbers on the *x*-axis indicate the chain
F11:2 length of *n*-alkanes.

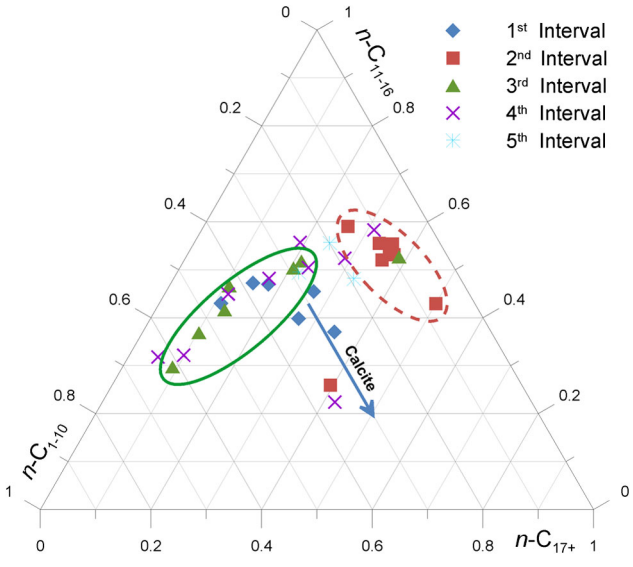


F12:1 **Figure 12.** Tvap-gas chromatography *n*-alkane distribution.
F12:2 Ternary diagram using the sum of *n*-$C_{1-10}$ versus *n*-$C_{11-16}$ versus
F12:3 *n*-$C_{17+}$ alkanes.

Hill et al., 2007a). Pr/*n*-$C_{17}$ and Ph/*n*-$C_{18}$ ratios are similar for all samples throughout the Marathon 1 Mesquite sequence with average values of 0.70 and 0.58, respectively (Figure 13B). This indicates a similar maturity level and source organic matter. Many well-known purely marine shales, including the Barnett Shale (Hill et al., 2007a), plot in the region the majority of Marathon 1 Mesquite samples plot in Figure 14. This region was demonstrated to be rather indicative of mixed anoxic, dysoxic depositional conditions than of a specific kerogen type. Only one sample from the false Barnett shows a composition more typical of an oxidizing depositional environment.

Thermal extract yields of monoaromatic hydrocarbons as well as di- and triaromatic hydrocarbons are illustrated in the depth profile of Figure 13C and D, respectively. Monoaromatics are concentrated in the organic-rich lower third and upper fourth intervals, whereas the concentration of diaromatics and especially triaromatics does not show a significant difference spanning the entire sequence. The distribution pattern of aromatics is documented to change with an increasing degree of maturity both under artificial and natural thermal conditions (Ishiwatari and Fukushima, 1979; Radke et al., 1982). Interestingly, Leythaeuser et al. (1988b) have shown that triaromatic hydrocarbons (phenanthrenes) seem not to have been affected by fractionation related to migration or expulsion. This also seems to be the case for samples from the Marathon 1 Mesquite because phenanthrene distribution patterns are similar throughout the well (Figure 13D, E). Thus, we have used the methylphenanthrene index (MPI) introduced by Radke et al. (1982) to assess the maturity of retained hydrocarbons:

$$\mathrm{MPI} - 1 = 1.5 \times [2\mathrm{MP} + 3\mathrm{MP}]/[\mathrm{P} + 1\mathrm{MP} + 9\mathrm{MP}]$$

$$\mathrm{Rc}\ (\%) = 0.60 \times \mathrm{MPI} - 1 + 0.40 \quad (\text{for } 0.65\% < \mathrm{Ro} < 1.35\%)$$

$$\mathrm{Rc}\ (\%) = -0.60 \times \mathrm{MPI} - 1 + 2.30 \quad (\text{for } 1.35\% < \mathrm{Ro} < 2.00\%)$$

where P, 1MP, 2MP, 3MP, and 9MP are the individual concentrations of phenanthrene, 1-, 2-, 3-, and 9-methylphenanthrenes, respectively; Rc is the calculated vitrinite reflectance.

The maturity of retained hydrocarbons calculated from the MPI (Rc % = 0.60 × MPI-1 + 0.40) is similar throughout the Marathon 1 Mesquite well and exhibits equivalent calculated vitrinite reflectance values approximately 1.02 Rc % (Figure 13F). This value is comparable to the $T_{max}$-derived maturity (~455°C [851°F], 1.03 Rc %) of kerogen especially in the most organic-rich third interval.

## Compositional Mass-Balance Calculation

Mass-balance models have been used for many years to calculate likely total oil and gas reserves on a regional scale. For example, Merewether and Claypool (1980) predicted the volumes of petroleum generated by Cretaceous source rocks in the Powder River Basin, Jones (1981) made similar calculations for other petroleum systems and was able to remark upon migration efficiency, whereas other groups (Pelet, 1985; Cooles et al., 1986) used simple algebraic schemes using Rock-Eval and TOC data for calculating not only masses of petroleum but also degrees of thermal transformation and expulsion efficiency. Santamaria-Orozco and Horsfield (2003) extended these principles to predict gas-oil ratios

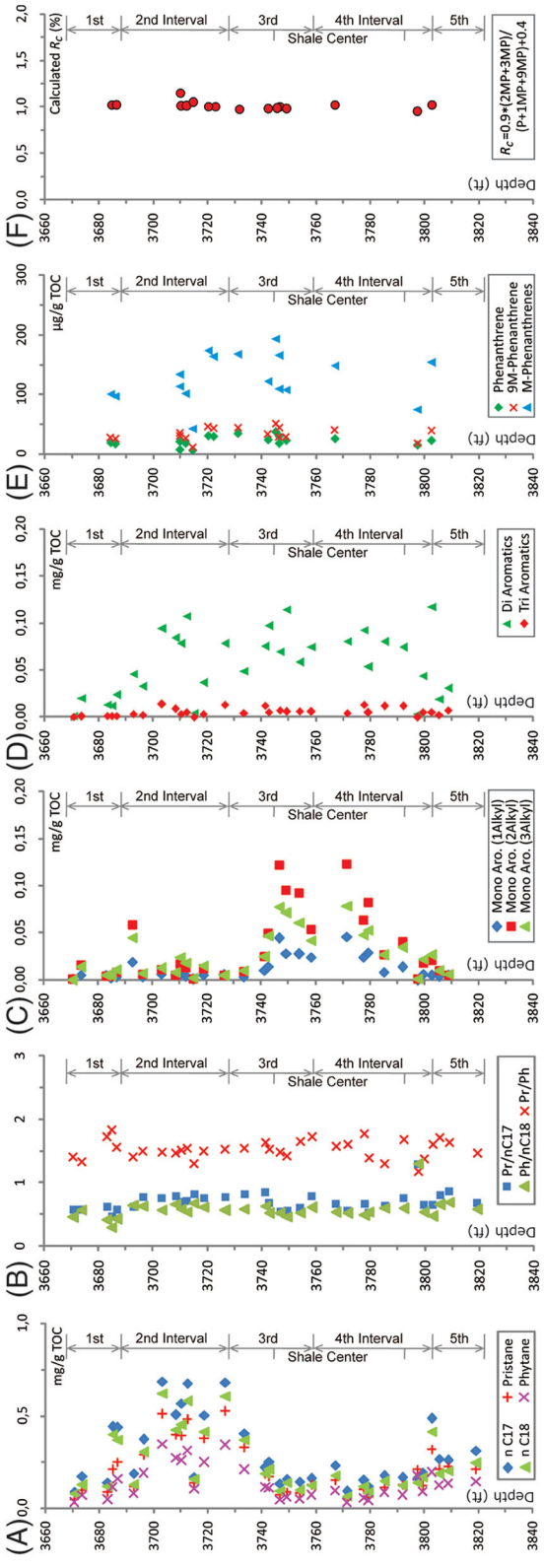


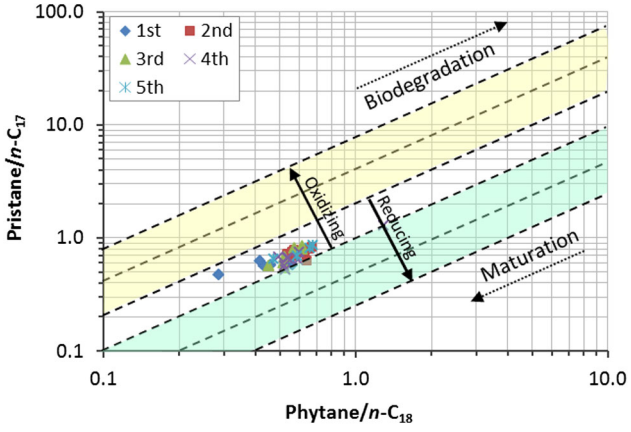


**Figure 14.** Tvap-gas chromatography pristane/$n$-$C_{17}$ versus phytane/$n$-$C_{18}$ for depositional environment typing. F14:1 F14:2

and other compositional attributes of petroleum using quantitative pyrolysis GC data: 869 870

$$\text{Step1: renormalization } N_i = [N_x \times (1200 - HI_o)]/(1200 - HI_x)$$

where $N_i$ is the initial concentration of any given component back calculated to its original $TOC_o$ (mg/g $TOC_o$), $N_x$ is the measured concentration normalized to the present TOC content (mg/g TOC), $HI_x$ = hydrogen index of mature sample as measured, and $HI_o$ = hydrogen index of immature sample; 1200 represents the reciprocal (times 1000) of 0.83, the assumed proportion of carbon in Rock-Eval pyrolysis products (Behar et al., 2001). 871 872 873 874 875 876 877 878 879

$$\text{Step2: subtraction } N_g = (N_o - N_i) \times [(N_x/N_i) \times \text{TOC}]$$

where $N_g$ (mg/g rock) is the concentration of generated hydrocarbon component. 880 881

The second interval is TOC leaner than the third interval, whereas its retained hydrocarbon content is highest of all intervals (Table 1 and Figure 2). Thus, a compositional mass-balance calculation has been 882 883 884 885

**Figure 13.** Tvap-gas chromatography (GC) and GC-mass spectroscopy geochemical depth profile. (A) Concentration of long-chain alkanes ($n$-$C_{17}$ and $n$-$C_{18}$) and isobranched alkanes (pristane and phytane). (B) Pristane and phytane ratios. (C) Concentration of monoaromatics. (D) Concentration of di and triaromatics. (E) Concentration of phenanthrene, 9-methylphenanthrene, and methylphenanthrenes. (F) Calculated vitrinite reflectance using the methylphenanthrene index. TOC = total organic carbon; MPI = methylphenanthrene index. F13:1 F13:2 F13:3 F13:4 F13:5 F13:6 F13:7 F13:8 F13:9

carried out to examine depletion and enrichment phenomena. Py-GC yields of one immature sample from the San Saba outcrop were used to define the original hydrocarbon generation potential of individual hydrocarbon compounds ($N_o$, mg/g $TOC_o$), whereas Py-GC yields of each mature sample from the Marathon 1 Mesquite well were used to define the residual hydrocarbon generation potential of individual hydrocarbon compounds ($N_x$, mg/g TOC). The concentration of compounds generated between those two maturity stages ($N_g$, mg/g rock) was then determined as above mentioned by simply subtracting the residual potential normalized to original $TOC_o$ ($N_i$, mg/g $TOC_o$) from the original potential $N_o$. For the least mature sample from the San Saba outcrop, renormalization is not necessary because its value $N_o$ represents the immature starting point with which all other samples are compared.

Here, $HI_x$ was used for the original $TOC_o$ renormalization procedure. Nevertheless and as previously shown, S2 values of unextracted samples are systematically overestimated (>14%), which also leads to an overestimation of the remaining generation potential $HI_x$; HI values are higher before Soxhlet extraction (Table 1). Thus, corrected HI values from extracted samples should be used for the mass-balance calculation, which actually also requires correction of TOC values. The correction of S2 value was achieved by applying the very good correlation $S2_{extracted} = 0.8551 \times S2_{unextracted} - 1.7179$ ($R^2 = 0.9401$) between that of extracted and unextracted samples (Figure 8A), whereas the correction of TOC was achieved by subtracting the amount of total oil (Total oil = $2.1556 \times S1$, $R^2 = 0.9158$; Figure 8C) from the TOC value of unextracted samples. Using those "carry-over" corrected HI* and TOC* values, the mass balance was recalculated (stippled lines, bars, symbols in Figures 15–17) and compared to uncorrected results (solid lines, bars, symbols in Figures 15–17).

By applying both methods, we computed the amount of individual *n*-alkanes that were generated by each sample. The average generated *n*-alkane concentrations of the entire Barnett Shale sequence are illustrated in Figure 15A. It can be seen that

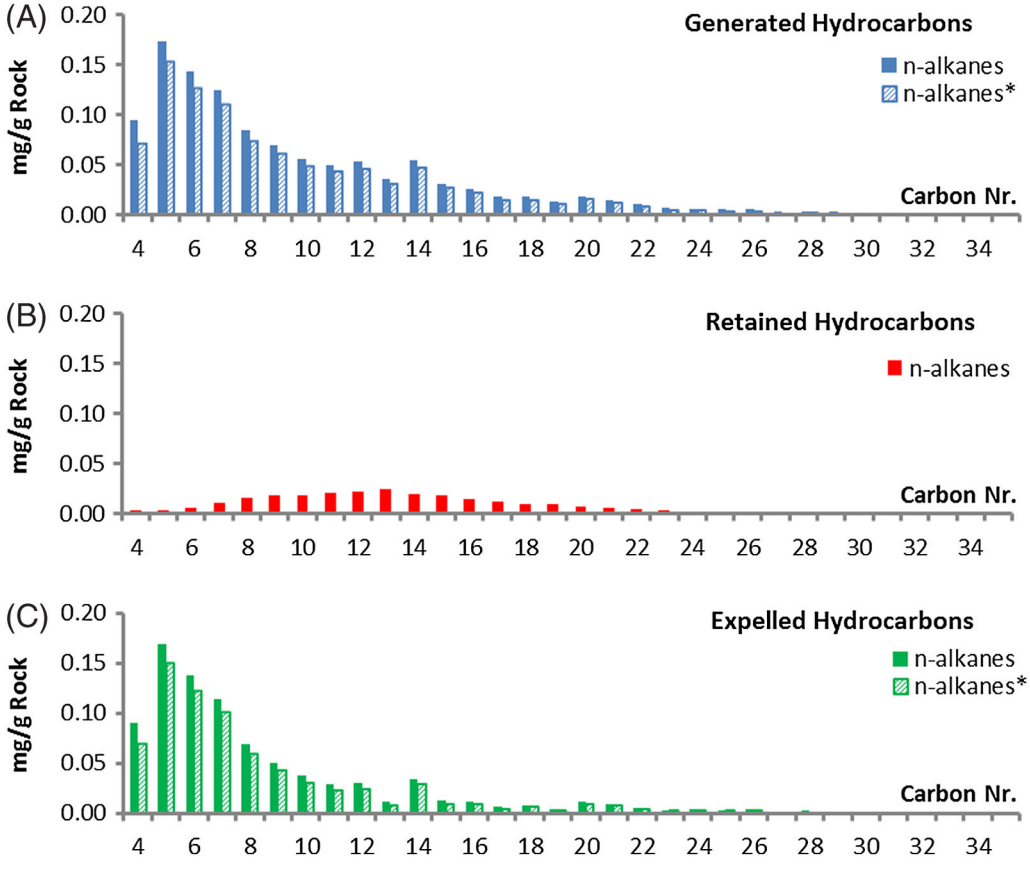


**Figure 15.** Compound-specific (*n*-alkanes) mass-balance calculation using the San Saba outcrop sample as the immature equivalent. (A) average amount of generated *n*-alkanes, (B) average amount of retained *n*-alkanes, (C) average amount of expelled *n*-alkanes up to the present maturity stages. Carry-over-corrected results using the corrected HI* and TOC* values are marked by an asterix (*). HI = hydrocarbon index; TOC = total organic carbon.

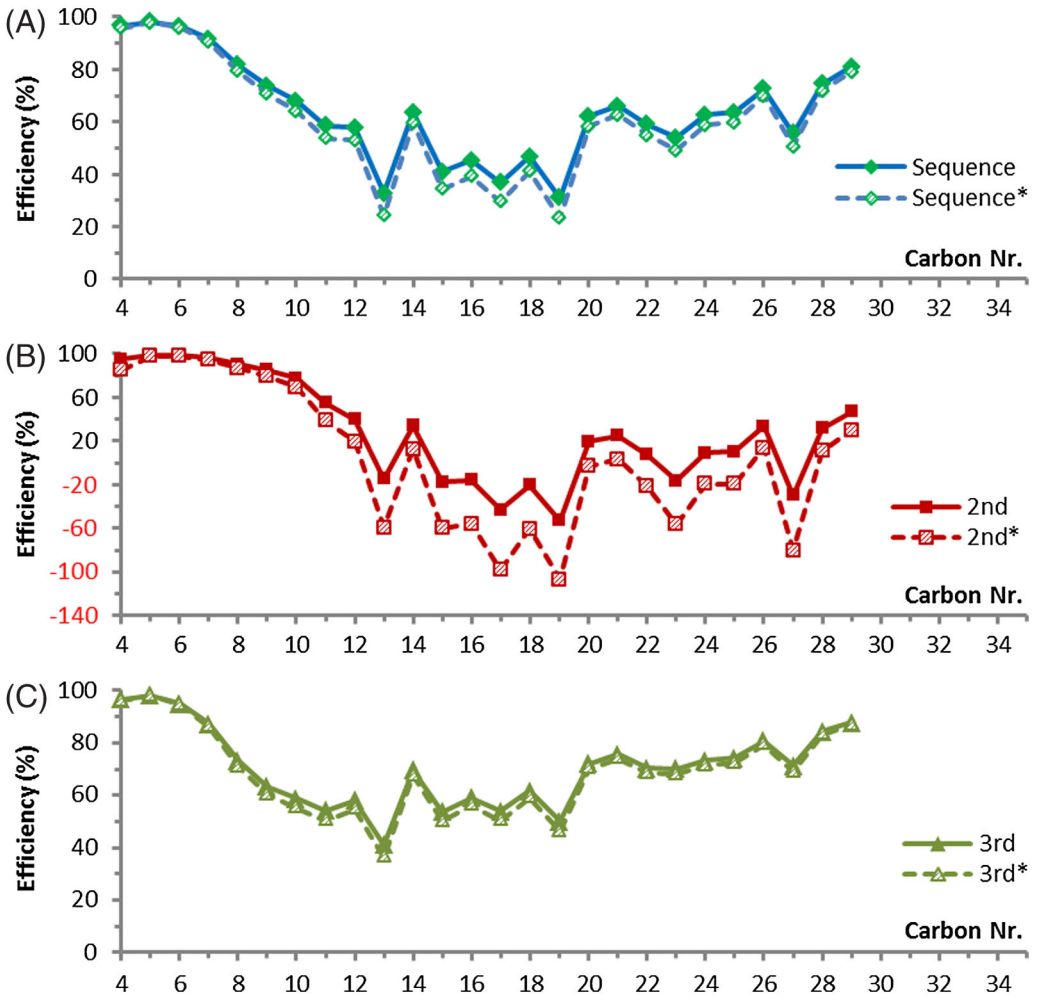


**Figure 16.** Compound-specific (*n*-alkanes) expulsion efficiency calculated by division of expelled *n*-alkanes and generated *n*-alkanes for (A) the entire Barnett Shale sequence, (B) the second interval, and (C) the third interval. Carry-over-corrected results using the corrected HI* and TOC* values are marked by an asterix (*). HI = hydrocarbon index; TOC = total organic carbon.

light-end oils dominate the generated hydrocarbons (gas hydrocarbons are not shown here), and *n*-$C_5$ has the highest concentration of all generated liquid *n*-alkanes. With increasing molecular weight, the concentrations of generated hydrocarbons gradually decrease to zero when approaching *n*-$C_{29}$. Average generated *n*-alkane concentrations are only slightly lower using the "carry-over" corrected mass balance.

After generation of hydrocarbons, petroleum migration/expulsion occurred under geologic conditions. The amount of expelled hydrocarbons can now be assessed by subtracting retained *n*-alkanes, as quantified by Tvap-GC (Figure 15B), from the calculated generated yields (Figure 15A). The calculated average amount of expelled hydrocarbons using the "carry-over" corrected and uncorrected mass balance is shown in Figure 15C. Concentrations are only slightly lower using the corrected mass balance whereas the distribution pattern is similar for both methods.

Based on the above data, expulsion efficiencies can be calculated for individual *n*-alkanes using the ratio of the concentration of expelled compound over the concentration of generated compound (times 100) (Figure 16). For samples of the entire Barnett Shale sequence, highest expulsion efficiency of 98% is calculated for *n*-alkanes up to $C_6$ (Figure 16A). As chain length increase, the calculated expulsion efficiency decreases to approximately 40% when approaching *n*-$C_{19}$, whereas it increases again and finally reaches 80% at *n*-$C_{29}$. The latter increase in expulsion efficiency is not geologically reasonable because long-chain alkanes should be less mobile (Mackenzie et al., 1983) and preferentially retained (Ritter, 2003). This phenomenon is most likely an artifact and possibly related to the previously discussed carry-over effect. Tvap-GC is performed isothermally at 300°C (572°F); thus, the $C_{19+}$ compounds are to some degree

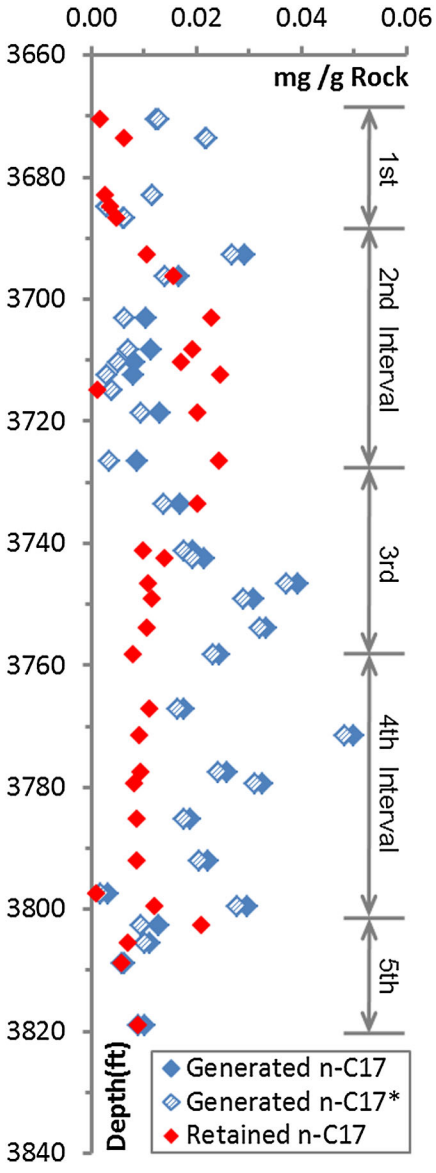


F17:1 **Figure 17.** Compound-specific ($n$-$C_{17}$) mass-balance calcula-
F17:2 tion using the San Saba outcrop sample as the immature equiv-
F17:3 alent for each sample showing generated $n$-$C_{17}$ and retained
F17:4 $n$-$C_{17}$. Carry-over-corrected results using the corrected HI* and
F17:5 TOC* values are marked by an asterix (*). HI = hydrocarbon
F17:6 index; TOC = total organic carbon.

968 incompletely vaporized. The concentration of
969 retained heavy-end compounds might therefore be
970 underestimated, and the degree of underestimation
971 increases for increasingly higher molecular weight
972 compounds. Thus, concentrations of expelled heavy
973 ends are overestimated, resulting in calculated
974 expulsion efficiencies that are too high for long-
**Q5** chain $n$-alkanes (Figure 16A). The carry-over effect
976 therefore not only influences the quantification of

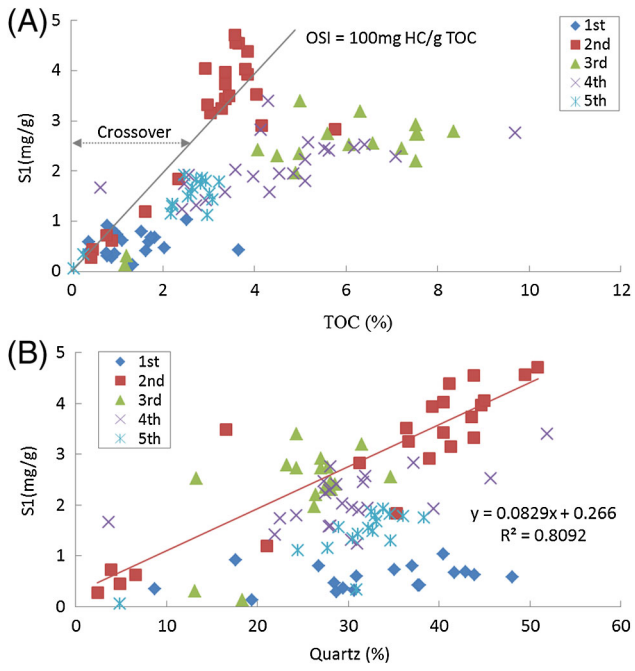


**Figure 18.** Controls on hydrocarbon retention are revealed by F18:1
plotting (A) S1 versus total organic carbon content and (B) S1 F18:2
versus quartz content. F18:3

977 retained hydrocarbons, but it also affects mass-
978 balance calculation results.

979 Expulsion efficiencies calculated for samples
980 exclusively from the second interval or third interval
981 are shown in Figure 16B and C, respectively.
982 Expulsion efficiencies calculated for the second inter-
983 val are negative for $n$-alkanes with more than 13
984 C-atoms. "Carry-over corrected" values are even
985 approximately 20% lower (stippled lines and sym-
986 bols). Negative expulsion efficiencies indicate that
987 more hydrocarbons are in place than could have been
988 generated from organic matter within the interval
989 itself, and additional hydrocarbons must have
990 migrated and accumulated therein. In contrast to the
991 second interval, expulsion efficiencies of the third
992 interval show only limited differences between uncor-
993 rected and "carry-over corrected" values (Figure 16C)
994 and resemble the signature observed for samples of the
995 whole sequence (Figure 16A). Expulsion efficiency is
996 highest at $n$-$C_5$ (98%), decreases to approximately
997 50% when approaching $n$-$C_{19}$ (which is 10% higher
998 than for samples of the entire sequence) and increases
999 again to approximately 90% at $n$-$C_{29}$. Assuming that
1000 no hydrocarbons migrated into and accumulated in
1001 the third interval, calculated expulsion efficiencies of

this interval can be treated as being correct for any given component under review. Nevertheless, for assessing how much has been expelled from the Barnett Shale in total, expulsion efficiencies considering the whole sequence (Figure 16A) have to be used, as some of the "expelled" hydrocarbons obviously accumulated within other Barnett Shale intervals, i.e., in our case the second interval.

Calculated concentrations of generated and retained $n$-$C_{17}$ are shown in a vertical profile for samples from all Marathon 1 Mesquite well intervals (Figure 17). $n$-$C_{17}$ is chosen as an example, because for intermediate molecular weight compounds, effects of either evaporative gas loss or "carryover" of heavy ends can be assumed to be the smallest. It becomes clear that, in contrast to samples from the first, third, fourth, and fifth interval, most samples from the second interval retain more $n$-$C_{17}$ than they could have been generated at present maturity levels (Figure 17). Thus, the second interval can be described as a reservoir unit within the Barnett Shale succession, most likely sourced by the more organic-rich, underlying intervals.

# DISCUSSION

## Controls on Hydrocarbon Retention

There are principally two factors that exert control upon hydrocarbon retention: (1) organic matter properties, i.e., organic richness, kerogen type, thermal maturity, and organic-porosity and (2) inorganic characteristics, i.e., the mineral composition, porosity, permeability, fractures, cementation, pressure, etc.

It is now widely accepted that the solid organic matter can retain liquid petroleum mainly via absorption and/or adsorption (Pepper, 1992; Sandvik et al., 1992; Jarvie et al., 2007; Loucks et al., 2009). We have demonstrated that organic richness exerts a major control on hydrocarbon retention in our sample set, as illustrated by the correlation between hydrocarbon abundance (S1) and the TOC content (Figure 18A). We have also shown that biogenic quartz content is a controlling factor for stored hydrocarbons, but only in the second interval (trendline in Figure 18B). Adsorption on clays (Espitalie et al., 1980; Schettler and Parmely, 1991) appears to be of less importance: the third interval, richest in I-S, contains less petroleum (S1) than the quartz-dominated, siliceous second interval.

We here propose two empirical equations for describing the controls of hydrocarbon retention throughout the whole sequence:

$$S1^{cal} = 0.320 \times TOC + 0.062 \times Quartz - 0.007 \text{ for the second interval}$$

$$S1^{cal} = 0.331 \times TOC + 0.008 \times Quartz + 0.220 \text{ for other intervals}$$

where S1 is the Rock-Eval thermal extract yield (mg/g sample). TOC is the organic matter richness (wt. %), and quartz is the content derived from the ATR-FTIR measurement (wt. %). By applying these two equations, a good overall match ($R^2 = 0.829$) between calculated S1 values and measured S1 data was achieved (Figure 19A). In the regression equation of the second interval, the coefficient value

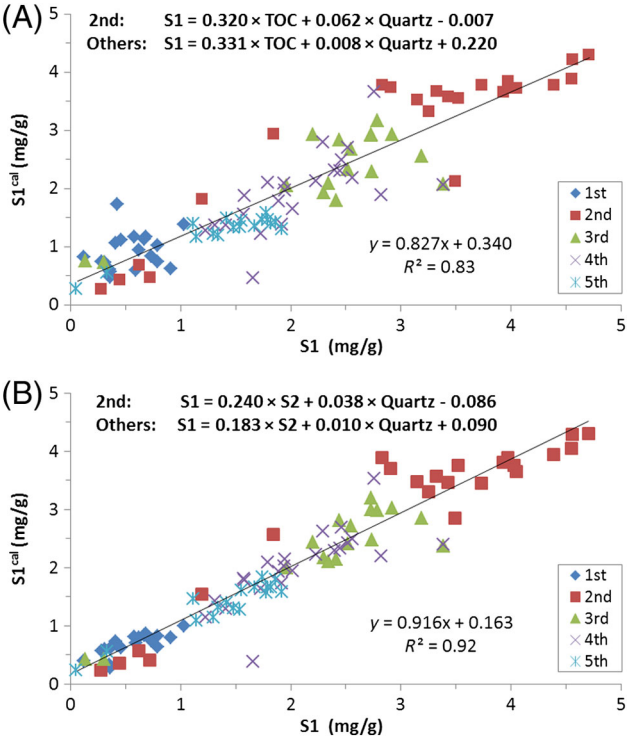


**Figure 19.** Calculated versus measured S1 values. The equations proposed in graph A describe the controls of organic richness (total organic carbon [TOC] wt. %) and quartz (wt. %) on hydrocarbon retention, whereas the equations proposed in graph B exclude the influence of inert kerogen by replacing TOC with S2.

of TOC is much larger than that of quartz (0.320 versus 0.062); thus, a stronger influence of organic matter on hydrocarbon retention is revealed. This is confirmed for other intervals as well (0.331 versus 0.008). Quartz exhibits a secondary influence on hydrocarbon storage for the second interval, as indicated by the relatively high coefficient value 0.062 in contrast to the coefficient value 0.008 for the other intervals. The latter coefficient value shows that quartz content itself indeed plays a very minor role, and it is even weaker than the uncertainty value (0.220).

Another finding, for application beyond the Barnett, is that labile or "live" carbon, and not simply the TOC, is the prime surface on which sorption takes place. In Figure 19, the parameter TOC (graph A) has been replaced by S2 (graph B) in the equations for the calculation of retained S1. An increased squared correlation coefficient ($R^2$) and the slope of the line approaching 1 indicate a better match between the computed and measured S1 values. Meanwhile, the *y*-intercept decreases from 0.340 to 0.163 indicating that the uncertainty of the equations is lower when inert kerogen is excluded from the equation. The importance of labile carbon composition as well as abundance in shales has only recently come to light. Mahlstedt and Horsfield (2013) have shown that the gradual aromatization of the labile kerogen component increases adsorptive potential and that some type II kerogens have enhanced adsorptive capacity over others because they are inherently more aromatic, even at low levels of maturity (e.g., Muscio and Horsfield, 1996).

## Petroleum Migration and Fractionation

Because organic matter within the studied Barnett Shale sequence possesses a rather homogenous kerogen type, compositionally similar petroleum should have been generated in all intervals upon thermal maturation. Variations in the composition of retained or stored bitumen/petroleum therefore have to be attributed to a migration fractionation effect related to preferential retention. In the Marathon 1 Mesquite well, when comparing the petroleum composition of samples from the organic-rich third interval ("source rock-unit") to samples from the organic-leaner second interval ("reservoir unit") (see Table 2 and Figure 10), the retained petroleum in the third interval is compositionally more aromatic and polar, whereas that in the second interval, it is more aliphatic. Confirmed by the higher, absolute concentration of aliphatic hydrocarbons within the second interval (Table 2), mass balance, and calculated expulsion efficiencies, these compositional differences are best explained by a preferential intrasource migration of aliphatic hydrocarbons from the organic-rich third interval into the second interval. Parts of the migrating petroleum were mixed with indigenously generated petroleum, resulting in a compositional dilution of aromatics and polars by aliphatic compounds. By division of the proportion of each fraction in the second and third interval (Table 2), the aliphatic-, aromatic-, resin-, and asphaltene-compound fractions of the second interval are specifically 1.41-, 0.83-, 0.65-, 0.43 times different than those of the third interval. Thus, a preferential retention sequence in the order polar compounds (asphaltenes > resins) > aromatic hydrocarbons > aliphatic hydrocarbons can be assigned, which is in line with data published in Leythaeuser et al. (1988c) and the experimental data of Sandvik et al. (1992).

In concordance with the study of Mackenzie et al. (1983), fractionation within alkanes can be observed in the Marathon 1 Mesquite well, with heavy-end *n*-alkanes being enriched in the second interval and lighter-end *n*-alkanes being enriched in the lower part of the third interval (Figure 11). The lower part of the third interval (major source "unit") thereby shows behavior as observed for the center of thick shale successions, whereas the second interval (reservoir-unit, but still "shale" and not sandstone) shows behavior as observed for the edge of those shale successions. It is certainly counterintuitive that light *n*-alkanes are said to preferentially migrate, but are still found in higher relative quantity in the third interval (shale center) than in the second interval (shale edge), into which we suggest petroleum migrated from the third interval. Nevertheless, an enrichment of migrated light *n*-alkanes within the second interval would have only taken place if petroleum migration had "stopped" therein. This was clearly not the case because calculated expulsion efficiencies for single hydrocarbons are very high in the second interval

for carbon numbers up to $n$-$C_{10}$ (Figure 16B), which is not completely explainable by evaporative gas loss. Calculated expulsion efficiencies only become negative for carbon numbers higher than $n$-$C_{12}$ indicating accumulation of additional liquid petroleum. Thus, it is very likely that especially the light hydrocarbons, presumably being more mobile, continued migration in a vertical or lateral direction (Mackenzie et al., 1983), leaving behind the heavier ones. This cannot be directly proved here because our study is restricted to 1-D movement of petroleum fluids (up and down the Marathon 1 Mesquite well), and detailed geochemical data from related conventional reservoirs were not acquired.

Phase separation is another possible scenario leading to molecular fractionation within compound classes. We observed clusters of oil inclusions in a carbonate-cemented fracture (Figure 5H, I), which is vertically elongated by approximately (91 m) (3 ft) in the core. According to Gale et al. (2007), high-angle fractures (>75°) filled by calcite are often observed within the Barnett Shale, and therefore they may act as an important migration pathway. The thin section visualizing the cemented fracture was picked parallel to a carbonate lamina (TOC = 0.87 wt. %) interbedded within relative organic-rich mudstone layers of the second interval. Phase separation induced by a sudden decrease in pressure during the opening of the fracture might have occurred during the primary migration process. According to Larter and Mills (1991), phase separation selectively "transfers" lower molecular weight hydrocarbons into the vapor phase. Then, after the release of the light vapor phase, the heavy-end liquid phase remains in the migration avenue and/or respective interval. It is conceivable, though very speculative, that migration associated with phase separation rather took place in the second interval than in the third interval, whereas timing and reasons remain unclear. The distribution of retained hydrocarbons would look more similar to the distribution of generated hydrocarbons when expulsion from the source proceeds without phase separation. This is actually the case when comparing the Tvap-GC $n$-alkane distribution pattern of samples from the lower third interval (Figure 11) to the distribution pattern of generated $n$-alkanes (Figure 15A). Concentrations decrease with increasing carbon number in both cases (when evaporative gas losses are taken into account for Tvap-GC). In contrast, for the second interval (and all other intervals), highest concentrations of thermally extractable $n$-alkanes are centered at $n$-$C_{13}$. This is more in line with the above-described effects of phase separation, i.e., heavy-end liquids remain and a light vapor phase was expelled.

We conclude that the intrasource migration process can alter the composition of petroleum fluids remaining in, and expelled from, the Barnett Shale in the Marathon 1 Mesquite well. Significant chemical fractionation between gross fractions occurs in the context of primary migration, whereas subtle differences within $n$-alkane distributions cannot be explained simply by molecular fractionation in a straightforward way. Migration is very likely to have occurred vertically according to all the above interpretations, but horizontal migration is not ruled out.

## CONCLUSION AND IMPLICATIONS

The analyzed oil window mature Barnett Shale sequence of the Marathon 1 Mesquite well, Hamilton County, Texas, has been subdivided top down into five discrete intervals. The first interval ("false" Barnett) actually corresponds to the calcite-rich and organic-lean Marble Falls Limestone. The second interval consists mainly of organic-rich noncalcareous mudstones, including porous biogenic silica from sponge spicules and behaves like a reservoir-unit within the succession. Highest free oil contents (S1) are observed here, causing oil crossovers, $T_{max}$ being shifted to lower values, and HI being shifted to higher values. The third interval is argillaceous and consists mainly of organic-rich siliceous noncalcareous mudstones and phosphatic shales. It represents the best source interval. The fourth and fifth intervals are calcite rich and consist mainly of siliceous calcareous mudstones.

The kerogen is rather homogenous throughout the Marathon 1 Mesquite well, indicating that compositionally similar petroleum was likely to have been generated upon thermal maturation. The HI values of approximately 200 mg HC/g TOC represent the remaining petroleum potential (Gas & Condensate to

P-N-A Low Wax Petroleum) of a type II kerogen at late oil window maturity (~1.0% $R_c$).

Compositional differences in gross chemical fractions of extracts, i.e., enrichment of aliphatic compounds in the second interval versus enrichment of aromatic hydrocarbons and especially polar compounds in the third interval, are best explained by a preferential migration of aliphatic hydrocarbons from the third into the second interval, or, in other words, by a preferential retention of polar compounds (asphaltenes > resins) > aromatic hydrocarbons > aliphatic hydrocarbon within the third interval. A vertical migration pathway can be deduced from the presence of carbonate-cemented fractures perpendicular to the bedding, as well as from the coexistence of oil inclusion clusters within these fractures. Molecular fractionation, i.e., a preferential expulsion of lower molecular weight hydrocarbons is also likely to occur during primary migration.

Empirical formulas indicate that matrix porosity acts as an important secondary storage mechanism for petroleum in the second interval. The retention of hydrocarbons within all other intervals is primarily controlled by organic matter richness, especially the "live" or "labile" component (S2), rather than TOC alone.

More hydrocarbons are present in the second interval than could have been generated by the kerogen during natural maturation, and excess petroleum has accumulated (reservoir unit). Estimates of just how much was expelled or retained are severely affected by the choice of sample material. We have demonstrated that (1) retained petroleum or "oil-in-place" is systematically (and minimally) underestimated by approximately 54% in these Barnett Shale samples when only S1 values from unextracted rock are considered, (2) the remaining generation potential is therefore systematically overestimated by at least 14% without extraction and correction, and (3) $T_{max}$ can be significantly shifted to lower values where carryover of S1 compounds into the S2 temperature range is strong in comparison with original TOC content and thus genetic potential (second interval). A more realistic assessment of total retained petroleum takes both the volatile and involatile petroleum components into account and uses the analysis of both extracted and unextracted samples.

The most important implication of the presented results is that the fluids in the siliceous second interval constitute a viable target. The lithology and oil quality at least resemble that found in conventional reservoir rocks or hybrid shale-oil systems. Improved oil quality (more aliphatic), added storage potential (sponge-spicule-derived microcrystalline quartz), and lower sorption affinities (of oil to organic matter) are present in the second interval in comparison to the third interval. Based on its overall mineral composition suggesting a high degree of brittleness, and taking frackability into account, the siliceous second interval is a much more attractive target for hydrocarbon production than the clay-rich and organic-rich third intervals. Furthermore, at higher maturities, the horizon is expected to yield higher additional amounts of secondary gas by oil cracking. This might explain why the primary producing facies of the Barnett Shale is volumetrically quartz dominated.

## REFERENCES CITED


Abouelresh, M. O., and R. M. Slatt, 2011, Shale depositional processes: Example from the Paleozoic Barnett Shale, Fort Worth Basin, Texas, USA: Open Geosciences, v. 3, no. 4, p. 398–409, doi:10.2478/s13533-011-0037-z.

Abouelresh, M. O., and R. M. Slatt, 2012, Lithofacies and sequence stratigraphy of the Barnett Shale in east-central Fort Worth Basin, Texas: AAPG Bulletin, v. 96, no. 1, p. 1–22, doi:10.1306/04261110116.

Adamu, M. B., 2012, Mineralogical and petrophysical characterisation of gas shale Colorado Group, Western Canada Sedimentary Basin: Ph.D. thesis, Newcastle University, Newcastle, United Kingdom, 218 p.

Arfaoui, A., and M. Montacer, 2007, New potential hydrocarbon source-rocks in the Lower Eocene Metlaoui Formation (Central-Northern Tunisia, Northern Africa): Geologica Acta, v. 5, no. 3, p. 245–254, doi:10.1344/105.000000297.

Baker, D. R., 1962, Organic geochemistry of Cherokee Group in southeastern Kansas and northeastern Oklahoma: AAPG Bulletin, v. 46, no. 9, p. 1621–1642.

Barker, C., 1974, Pyrolysis techniques for source-rock evaluation: AAPG Bulletin, v. 58, no. 11, p. 2349–2361.

Behar, F., V. Beaumont, and H. L. De B. Penteado, 2001, Rock-Eval 6 technology: Performances and developments: Oil & Gas Science and Technology—Revue de l'IFP, v. 56, no. 2, p. 111–134, doi:10.2516/ogst:2001013.

Bernard, S., and B. Horsfield, 2014, Thermal maturation of gas shale systems: Annual Review of Earth and Planetary Sciences, v. 42, no. 1, p. 635–651, doi:10.1146/annurev-earth-060313-054850.

Bernard, S., R. Wirth, A. Schreiber, H.-M. Schulz, and B. Horsfield, 2012, Formation of nanoporous pyrobitumen residues during maturation of the Barnett Shale (Fort Worth Basin): International Journal of Coal Geology, v. 103, p. 3–11, doi:10.1016/j.coal.2012.04.010.

Bernhard, J. M., 1989, The distribution of benthic foraminifera with respect to oxygen concentration and organic carbon levels in shallow-water Antarctic sediments: Limnology and Oceanography, v. 34, no. 6, p. 1131–1141.

Bowker, K. A., 2003, Recent development of the Barnett Shale play, Fort Worth basin: West Texas Geological Society Bulletin, v. 42, no. 6, p. 4–11.

Bowker, K. A., 2007, Barnett Shale gas production, Fort Worth Basin: Issues and discussion: AAPG Bulletin, v. 91, no. 4, p. 523–533, doi:10.1306/06190606018.

Brenneman, M. C., and P. V. Smith Jr., 1958, The chemical relationships between crude oils and their source rocks, *in* L. G. Weeks, ed., Habitat of oil: A symposium: Tulsa, Oklahoma, AAPG, p. 818–849.

Brooks, J. D., K. Gould, and J. W. Smith, 1969, Isoprenoid hydrocarbons in coal and petroleum: Nature, v. 222, no. 5190, p. 257–259.

Bunting, P. J., and J. A. Breyer, 2012, Extended abstract—Lithology of the Barnett Shale (Mississippian), Southern Fort Worth Basin, Texas, *in* J. A. Breyer, ed., Shale reservoirs—Giant resources for the 21st century: AAPG Memoir 97, p. 35–39.

Claypool, G. E., and P. R. Reed, 1976, Thermal-analysis technique for source-rock evaluation: Quantitative estimate of organic richness and effects of lithologic variation: AAPG Bulletin, v. 60, no. 4, p. 608–626.

Clementz, D. M., 1979, Effect of oil and bitumen saturation on source-rock pyrolysis: AAPG Bulletin, v. 63, no. 12, p. 2227–2232.

Cooles, G. P., A. S. Mackenzie, and T. M. Quigley, 1986, Calculation of petroleum masses generated and expelled from source rocks: Organic Geochemistry, v. 10, no. 1–3, p. 235–245, doi:10.1016/0146-6380(86)90026-4.

Dembicki, H. J., B. Horsfield, and T. T. Y. Ho, 1983, Source rock evaluation by pyrolysis-gas chromatography: AAPG Bulletin, v. 67, no. 7, p. 1094–1103.

Di Primio, R., and B. Horsfield, 1996, Predicting the generation of heavy oils in carbonate/evaporitic environments using pyrolysis methods: Organic Geochemistry, v. 24, no. 10–11, p. 999–1016, doi:10.1016/S0146-6380(96)00116-7.

Didyk, B. M., B. R. T. Simoneit, S. C. Brassell, and G. Eglinton, 1978, Organic geochemical indicators of palaeoenvironmental conditions of sedimentation: Nature, v. 272, no. 5650, p. 216–222.

Eglinton, T. I., J. S. Sinninghe Damsté, M. E. L. Kohnen, and J. W. de Leeuw, 1990, Rapid estimation of the organic sulphur content of kerogens, coals and asphaltenes by pyrolysis-gas chromatography: Fuel, v. 69, no. 11, p. 1394–1404, doi:10.1016/0016-2361(90)90121-6.

Q6 EOG Resources, 2010, Annual report, http://www.eogresources.com/investors/reports/2010/EOGR_2010_Annual_Report.pdf.

Q7 EOG Resources, 2013, Investor presentation, http://blog.mysanantonio.com/eagle-ford-fix/files/2013/02/EOG.pdf.

Eseme, E., R. Littke, B. M. Krooss, and J. Schwarzbauer, 2007, Experimental investigation of the compositional variation of petroleum during primary migration: Organic Geochemistry, v. 38, no. 8, p. 1373–1397, doi:10.1016/j.orggeochem.2007.03.003.

Espitalie, J., M. Madec, and B. Tissot, 1980, Role of mineral matrix in kerogen pyrolysis: Influence on petroleum generation and migration: AAPG Bulletin, v. 64, no. 1, p. 59–66.

Espitalie, J., M. Madec, B. Tissot, J. J. Mennig, and P. Leplat, Q8 1977, Source rock characterization method for petroleum exploration: Offshore Technology Conference, Houston, Texas, p. 439–444.

Gale, J. F. W., R. M. Reed, and J. Holder, 2007, Natural fractures in the Barnett Shale and their importance for hydraulic fracture treatments: AAPG Bulletin, v. 91, no. 4, p. 603–622, doi:10.1306/11010606061.

Gooday, A. J., 1994, The biology of deep-sea foraminifera: A review of some advances and their applications in paleoceanography: Palaios, v. 9, no. 1, p. 14–31, doi:10.2307/3515075.

Haberer, R. M., K. Mangelsdorf, H. Wilkes, and B. Horsfield, 2006, Occurrence and palaeoenvironmental significance of aromatic hydrocarbon biomarkers in Oligocene sediments from the Mallik 5L-38 Gas Hydrate Production Research Well (Canada): Organic Geochemistry, v. 37, no. 5, p. 519–538, doi:10.1016/j.orggeochem.2006.01.004.

Hickey, J. J., and B. Henk, 2007, Lithofacies summary of the Mississippian Barnett Shale, Mitchell 2 T.P. Sims well, Wise County, Texas: AAPG Bulletin, v. 91, no. 4, p. 437–443, doi:10.1306/12040606053.

Hill, R. J., D. M. Jarvie, J. Zumberge, M. Henry, and R. M. Pollastro, 2007a, Oil and gas geochemistry and petroleum systems of the Fort Worth Basin: AAPG Bulletin, v. 91, no. 4, p. 445–473, doi:10.1306/11030606014.

Hill, R. J., E. Zhang, B. J. Katz, and Y. Tang, 2007b, Modeling of gas generation from the Barnett Shale, Fort Worth Basin, Texas: AAPG Bulletin, v. 91, no. 4, p. 501–521, doi:10.1306/12060606063.

Horsfield, B., 1989, Practical criteria for classifying kerogens: Some observations from pyrolysis-gas chromatography: Geochimica et Cosmochimica Acta, v. 53, no. 4, p. 891–901, doi:10.1016/0016-7037(89)90033-1.

Horsfield, B., S. Bharati, S. R. Larter, F. Leistner, R. Littke, H. J. Schenk, and H. Dypvik, 1992, On the atypical petroleum-generating characteristics of alginite in the Cambrian Alum Shale, *in* M. Schidlowski, ed., Early organic evolution: Implications for mineral and energy resources: Berlin, Germany, Springer-Verlag, p. 257–266.

Horsfield, B., H. Dembicki, and T. T. Y. Ho, 1983, Some potential applications of pyrolysis to basin studies: Journal of the Geological Society, v. 140, no. 3, p. 431–443, doi:10.1144/gsjgs.140.3.0431.

Horsfield, B., F. Leistner, and K. Hall, 2015, Microscale sealed vessel pyrolysis, *in* K. Grice, ed., Principles and practice of analytical techniques in geosciences: Royal Society of Chemistry Detection Science Series 4, p. 209–250.

Ishiwatari, R., and K. Fukushima, 1979, Generation of unsaturated and aromatic hydrocarbons by thermal alteration of

young kerogen: Geochimica et Cosmochimica Acta, v. 43, no. 8, p. 1343–1349, doi:10.1016/0016-7037(79)90124-8.

Jarvie, D. M., 2012, Shale resource systems for oil and gas: Part 2—Shale-oil resource systems, *in* J. A. Breye, ed., Shale reservoirs—Giant resources for the 21st century: AAPG Memoir 97, p. 89–119.

Jarvie, D. M., 2014, Components and processes affecting producibility and commerciality of shale resource systems: Geologica Acta, v. 12, no. 4, p. 307–325, doi:10.1344/GeologicaActa2014.12.4.3.

Jarvie, D. M., and D. R. Baker, 1984, Application of the Rock-Eval III Oil Show Analyzer to the study of gaseous hydrocarbons in an Oklahoma gas well: 187th American Chemical Society National Meeting, 21 p.

Jarvie, D. M., B. Claxton, B. Henk, and J. Breyer, 2001a, Oil and shale gas from Barnett Shale, Ft. Worth Basin, Texas: AAPG National Convention.

Jarvie, D. M., R. J. Hill, and R. M. Pollastro, 2005, Assessment of the gas potential and yields from shales: The Barnett Shale model, *in* B. J. Cardott, ed., Unconventional energy resources in the southern Midcontinent, 2004 symposium: Oklahoma Geological Survey Circular 110, p. 37–50.

Jarvie, D. M., R. J. Hill, T. E. Ruble, and R. M. Pollastro, 2007, Unconventional shale-gas systems: The Mississippian Barnett Shale of north-central Texas as one model for thermogenic shale-gas assessment: AAPG Bulletin, v. 91, no. 4, p. 475–499, doi:10.1306/12190606068.

Jarvie, D. M., A. Morelos, and Z. Han, 2001b, Detection of pay zones and pay quality, Gulf of Mexico: Application of geochemical techniques: Gulf Coast Association of Geological Societies Transactions, v. 51, p. 151–160.

Jones, R. W., 1981, Some mass balance and geological constraints on migration mechanisms: AAPG Bulletin, v. 65, no. 1, p. 103–122.

Kelemen, S. R., C. C. Walters, D. Ertas, H. Freund, and D. J. Curry, 2006, Petroleum expulsion Part 3. A model of chemically driven fractionation during expulsion of petroleum from kerogen: Energy and Fuels, v. 20, no. 1, p. 309–319, doi:10.1021/ef058023s.

Keym, M., V. Dieckmann, B. Horsfield, M. Erdmann, R. Galimberti, L.-C. Kua, L. Leith, and O. Podlaha, 2006, Source rock heterogeneity of the Upper Jurassic Draupne Formation, North Viking Graben, and its relevance to petroleum generation studies: Organic Geochemistry, v. 37, no. 2, p. 220–243, doi:10.1016/j.orggeochem.2005.08.023.

Kruge, M. A., 1983, Diagenesis of Miocene biogenic sediments in Lost Hills Oil Field, San Joaquin Basin, California, *in* C. M. Isaacs and R. E. Garrison, eds., Petroleum generation and occurrence in the Miocene Monterey Formation, California: Los Angeles, California, Pacific Section, SEPM, p. 39–51.

Lafargue, E., J. Espitalie, T. Jacobsen, and S. Eggen, 1990, Experimental simulation of hydrocarbon expulsion: Organic Geochemistry, v. 16, no. 1–3, p. 121–131, doi:10.1016/0146-6380(90)90032-U.

Langford, F. F., and M. M. Blanc-Valleron, 1990, Interpreting Rock-Eval pyrolysis data using graphs of pyrolizable hydrocarbons vs. total organic carbon: AAPG Bulletin, v. 74, no. 6, p. 799–804.

Larter, S., 1988, Some pragmatic perspectives in source rock geochemistry: Marine and Petroleum Geology, v. 5, no. 3, p. 194–204, doi:10.1016/0264-8172(88)90001-3.

Larter, S., and N. Mills, 1991, Phase-controlled molecular fractionations in migrating petroleum charges, *in* W. A. England and A. J. Fleet, eds., Petroleum migration: Geological Society, London, Special Publications, v. 59, p. 137–147, doi:10.1144/gsl.sp.1991.059.01.10.

Leythaeuser, D., R. Littke, M. Radke, and R. G. Schaefer, 1988a, Geochemical effects of petroleum migration and expulsion from Toarcian source rocks in the Hils syncline area, NW-Germany: Organic Geochemistry, v. 13, no. 1–3, p. 489–502, doi:10.1016/0146-6380(88)90070-8.

Leythaeuser, D., M. Radke, and R. G. Schaefer, 1984, Efficiency of petroleum expulsion from shale source rocks: Nature, v. 311, no. 5988, p. 745–748.

Leythaeuser, D., M. Radke, and H. Willsch, 1988b, Geochemical effects of primary migration of petroleum in Kimmeridge source rocks from Brae field area, North Sea. II: Molecular composition of alkylated naphthalenes, phenanthrenes, benzo- and dibenzothiophenes: Geochimica et Cosmochimica Acta, v. 52, no. 12, p. 2879–2891, doi:10.1016/0016-7037(88)90155-X.

Leythaeuser, D., R. G. Schaefer, and M. Radke, 1988c, Geochemical effects of primary migration of petroleum in Kimmeridge source rocks from Brae field area, North Sea. I: Gross composition of $C_{15+}$-soluble organic matter and molecular composition of $C_{15+}$-saturated hydrocarbons: Geochimica et Cosmochimica Acta, v. 52, no. 3, p. 701–713, doi:10.1016/0016-7037(88)90331-6.

Loucks, R. G., R. M. Reed, S. C. Ruppel, and D. M. Jarvie, 2009, Morphology, genesis, and distribution of nanometer-scale pores in siliceous mudstones of the Mississippian Barnett Shale: Journal of Sedimentary Research, v. 79, no. 12, p. 848–861.

Loucks, R. G., and S. C. Ruppel, 2007, Mississippian Barnett Shale: Lithofacies and depositional setting of a deep-water shale-gas succession in the Fort Worth Basin, Texas: AAPG Bulletin, v. 91, no. 4, p. 579–601, doi:10.1306/11020606059.

Mackenzie, A. S., D. Leythaeuser, R. G. Schaefer, and M. Bjoroy, 1983, Expulsion of petroleum hydrocarbons from shale source rocks: Nature, v. 301, no. 5900, p. 506–509.

Mahlstedt, N., and B. Horsfield, 2013, A new screening tool for the rapid evaluation of gas sorption capacity in shales: AAPG Hedberg Conference, Beijing, China.

Martineau, D. F., 2007, History of the Newark East field and the Barnett Shale as a gas reservoir: AAPG Bulletin, v. 91, no. 4, p. 399–403, doi:10.1306/intro910407.

Merewether, E. A., and G. E. Claypool, 1980, Organic composition of some Upper Cretaceous Shale, Powder River Basin, Wyoming: AAPG Bulletin, v. 64, no. 4, p. 488–500.

Milliken, K., S.-J. Choh, P. Papazis, and J. Schieber, 2007, "Cherty" stringers in the Barnett Shale are agglutinated foraminifera: Sedimentary Geology, v. 198, no. 3–4, p. 221–232, doi:10.1016/j.sedgeo.2006.12.012.

Milliken, K. L., W. L. Esch, R. M. Reed, and T. Zhang, 2012, Grain assemblages and strong diagenetic overprinting in

siliceous mudrocks, Barnett Shale (Mississippian), Fort Worth Basin, Texas: AAPG Bulletin, v. 96, no. 8, p. 1553–1578, doi:10.1306/12011111129.

Muscio, G. P. A., and B. Horsfield, 1996, Neoformation of inert carbon during the natural maturation of a marine source rock: Bakken Shale, Williston Basin: Energy and Fuels, v. 10, no. 1, p. 10–18.

Muscio, G. P. A., B. Horsfield, and D. H. Welte, 1994, Occurrence of thermogenic gas in the immature zone—Implications from the Bakken in-source reservoir system: Organic Geochemistry, v. 22, no. 3–5, p. 461–476, doi:10.1016/0146-6380(94)90119-8.

Nicot, J.-P., B. R. Scanlon, R. C. Reedy, and R. A. Costley, 2014, Source and fate of hydraulic fracturing water in the Barnett Shale: A historical perspective: Environmental Science and Technology, v. 48, no. 4, p. 2464–2471, doi:10.1021/es404050r.

Papazis, P. K., and K. Milliken, 2005, Cathodoluminescent textures and the origin of quartz in the Mississippian Barnett Shale, Fort Worth Basin, Texas: AAPG Annual Convention.

Pelet, R., 1985, Evaluation quantitative des produits formés lors de l'évolution géochimique de la matière organique (in French): Oil & Gas Science and Technology, v. 40, no. 5, p. 551–562.

Pepper, A. S., 1992, Estimating the petroleum expulsion behaviour of source rocks: A novel quantitative approach, *in* W. A. England and A. J. Fleet, eds., Petroleum migration: Geological Society, London, Special Publications, v. 59, p. 9–31, doi:10.1144/gsl.sp.1991.059.01.02.

Pepper, A. S., and P. J. Corvi, 1995, Simple kinetic models of petroleum formation. Part I: Oil and gas generation from kerogen: Marine and Petroleum Geology, v. 12, p. 291–319.

Peters, K. E., 1986, Guidelines for evaluating petroleum source rock using programmed pyrolysis: AAPG Bulletin, v. 70, no. 3, p. 318–329.

Peters, K. E., T. H. Fraser, W. Amris, B. Rustanto, and E. Hermanto, 1999, Geochemistry of crude oils from eastern Indonesia: AAPG Bulletin, v. 83, no. 12, p. 1927–1942.

Pollastro, R. M., D. M. Jarvie, R. J. Hill, and C. W. Adams, 2007, Geologic framework of the Mississippian Barnett Shale, Barnett-Paleozoic total petroleum system, Bend arch–Fort Worth Basin, Texas: AAPG Bulletin, v. 91, no. 4, p. 405–436, doi:10.1306/10300606008.

Powell, T. G., and D. M. McKirdy, 1973, Relationship between ratio of pristane to phytane, crude oil composition and geological environment in Australia: Nature Physical Science, v. 243, p. 37–39.

Powell, T. G., H. L. Ten Haven, J. Rullkotter, J. W. De Leeuw, and J. S. S. Damste, 1988, Pristane/phytane ratio as environmental indicator: Nature, v. 333, no. 6174, p. 604–604.

Radke, M., D. H. Welte, and H. Willsch, 1982, Geochemical study on a well in the Western Canada Basin: Relation of the aromatic distribution pattern to maturity of organic matter: Geochimica et Cosmochimica Acta, v. 46, no. 1, p. 1–10, doi:10.1016/0016-7037(82)90285-X.

Radke, M., H. Willsch, and D. H. Welte, 1980, Preparative hydrocarbon group type determination by automated medium pressure liquid chromatography: Analytical Chemistry, v. 52, no. 3, p. 406–411, doi:10.1021/ac50053a009.

Ritter, U., 2003, Solubility of petroleum compounds in kerogen: Implications for petroleum expulsion: Organic Geochemistry, v. 34, no. 3, p. 319–326, doi:10.1016/S0146-6380(02)00245-0.

Romero-Sarmiento, M.-F., J.-N. Rouzaud, S. Bernard, D. Deldicque, M. Thomas, and R. Littke, 2014, Evolution of Barnett Shale organic carbon structure and nanostructure with increasing maturation: Organic Geochemistry, v. 71, p. 7–16, doi:10.1016/j.orggeochem.2014.03.008.

Sandvik, E. I., W. A. Young, and D. J. Curry, 1992, Expulsion from hydrocarbon sources: The role of organic absorption: Organic Geochemistry, v. 19, no. 1–3, p. 77–87, doi:10.1016/0146-6380(92)90028-V.

Santamaria-Orozco, D., and B. Horsfield, 2003, Gas generation potential of upper Jurassic (Tithonian) source rocks in the Sonda de Campeche, Mexico, *in* R. Bartolini, T. Buffler, and J. Blickwede, eds., The Circum-Gulf of Mexico and the Caribbean: Hydrocarbon habitats, basin formation, and plate tectonics: AAPG Memoir 79, p. 349–363.

Schettler, P. D., Jr., and C. R. Parmely, 1991, Contributions to total storage capacity in Devonian shales: SPE Eastern Regional Meeting, Lexington, Kentucky, October 22–25, 1991, SPE Paper 23422, p. 77–88, doi:10.2118/23422-MS.

Schieber, J., D. Krinsley, and L. Riciputi, 2000, Diagenetic origin of quartz silt in mudstones and implications for silica cycling: Nature, v. 406, no. 6799, p. 981–985.

Singh, P., 2008, Lithofacies and sequence stratigraphic framework of the Barnett Shale, Northeast Texas: Ph.D. thesis, The University of Oklahoma, Norman, Oklahoma, 181 p.

Slatt, R. M., and N. R. O. Brien, 2011, Pore types in the Barnett and Woodford gas shales: Contribution to understanding gas storage and migration pathways in fine-grained rocks: AAPG Bulletin, v. 95, no. 12, p. 2017–2030.

Soxhlet, F., 1879, Die gewichtsanalytische Bestimmung des Milchfettes (in German): Polytechnisches Journal, v. 232, p. 461–465.

Texas-RRC, 2015, Railroad Commission of Texas, http://www.rrc.state.tx.us/media/22205/barnettshale_oil_bblperday.pdf.

Theuerkorn, K., B. Horsfield, H. Wilkes, R. di Primio, and E. Lehne, 2008, A reproducible and linear method for separating asphaltenes from crude oil: Organic Geochemistry, v. 39, no. 8, p. 929–934, doi:10.1016/j.orggeochem.2008.02.009.

Tissot, B. P., and D. H. Welte, 1984, Petroleum formation and occurrence: Berlin, Germany, Springer-Verlag, 699 p.

# Queries

Q1. AU: Please check and confirm whether the running foot has been set correctly.

Q2. AU: Please check and confirm whether all the author's affiliations and email address have been set correctly.

Q3. AU: Please note that there are two references Hill et al., 2007a, 2007b in the references list. So, kindly mention whether the reference citation Hill et al., 2007 is either Hill et al., 2007a or Hill et al., 2007b which is cited in the caption of Figure 1.

Q4. AU: Please define API.

Q5. AU: Please confirm the sentence, "Thus, concentrations of expelled heavy ends are overestimated, resulting in calculated expulsion efficiencies that are too high for long-chain n-alkanes…."

Q6. AU: Please provide the accessed date ("Month Date, Year" in spell out form) for the last time you have accessed this website for reference "EOG Resources, 2010".

Q7. AU: Please provide the accessed date ("Month Date, Year" in spell out form) for the last time you have accessed this website for reference "EOG Resources, 2013".

Q8. AU: Please provide conference date (i.e., "Month Date, Year" in spell out form) details for reference Espitalie et al., 1977.

Q9. AU: Please provide conference location and conference date (i.e., "Month Date, Year" in spell out form) details for reference Jarvie and Baker, 1984.

Q10. AU: Please provide conference location, conference date (i.e., "Month Date, Year" in spell out form) details, and page range (or total number of pages) for reference Jarvie et al., 2001a.

Q11. AU: Please provide conference date (i.e., "Month Date, Year" in spell out form) details and page range (or total number of pages) for reference Mahlstedt and Horsfield, 2013.

Q12. AU: Please provide conference location, conference date (i.e., "Month Date, Year" in spell out form) details, and page range (or total number of pages) for reference Papazis and Milliken, 2005.

Q13. AU: Please provide the accessed date ("Month Date, Year" in spell out form) for the last time you have accessed this website for reference Texas-RRC, 2015.